Journal Pre-proof

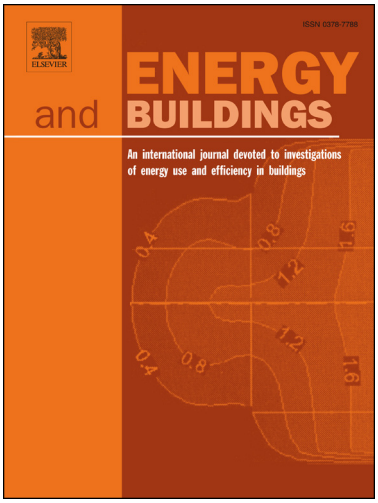

Evaluation of a Kirigami-Inspired Double-Skin Adaptive Façade for Natural Ventilation and Solar Harvesting to Enhance Indoor Environment and Energy Performance

Rodrigo Arauz, Evgeni Filipov, Alessandro Fascetti, Dale T. Clifford and John C. Brigham

PII: S0378-7788(24)01043-0
DOI: https://doi.org/10.1016/j.enbuild.2024.114927
Reference: ENB 114927

To appear in: *Energy & Buildings*

Received date: 27 June 2024
Revised date: 8 October 2024
Accepted date: 15 October 2024

Please cite this article as: R. Arauz, E. Filipov, A. Fascetti et al., Evaluation of a Kirigami-Inspired Double-Skin Adaptive Façade for Natural Ventilation and Solar Harvesting to Enhance Indoor Environment and Energy Performance, *Energy & Buildings*, 114927, doi: https://doi.org/10.1016/j.enbuild.2024.114927.

Graphical abstract

Energy & Buildings ●●●●, ●●●, ●●●

Evaluation of a Kirigami-Inspired Double-Skin Adaptive Façade for Natural Ventilation and Solar Harvesting to Enhance Indoor Environment and Energy Performance

Rodrigo Arauz[a,*], Evgeni Filipov[b], Alessandro Fascetti[a], Dale T. Clifford[c], John C. Brigham[a]

[a] *Civil and Environmental Engineering, University of Pittsburgh, Pittsburgh, 15261, PA, United States*
[b] *Civil and Environmental Engineering, University of Michigan, Ann Arbor, 48109, MI, United States*
[c] *College of Architecture and Environmental Design, California Polytechnic State University, San Luis Obispo, 93405, CA, United States*

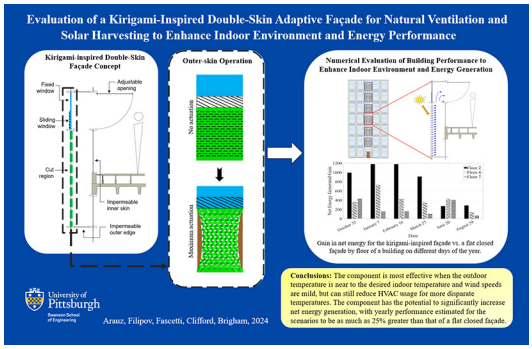

Highlights

- A novel concept for a kirigami-inspired double skin adaptive facade is introduced.
- The facade concept can reduce HVAC use, aid ventilation, and improve solar tracking.
- The façade can improve environmental performance for many varying conditions.

Evaluation of a Kirigami-Inspired Double-Skin Adaptive Façade for Natural Ventilation and Solar Harvesting to Enhance Indoor Environment and Energy Performance

Rodrigo Arauz[a,*], Evgeni Filipov[b], Alessandro Fascetti[a], Dale T. Clifford[c], John C. Brigham[a]

[a] *Civil and Environmental Engineering, University of Pittsburgh, Pittsburgh, 15261, Pennsylvania, United States*
[b] *Civil and Environmental Engineering, University of Michigan, Ann Arbor, 48109, Michigan, United States*
[c] *College of Architecture and Environmental Design, California Polytechnic State University, San Luis Obispo, 93405, California, United States*

Abstract

A novel kirigami-inspired design concept for an environmentally responsive adaptive façade is presented and evaluated for the objectives of solar energy harvesting and adaptive ventilation through controllable surface orientation and opening. The concept is a double-skin façade where the outer skin includes a straight cut kirigami-inspired adaptive component. Controllable actuation of the kirigami-inspired section opens the outer skin for ventilation while also changing the orientation of the outer surface for solar tracking. The primary objective of this study is to evaluate the potential benefits for this concept integrated within a building façade for solar energy harvesting, air changes, and indoor temperature control. As such, a computational study is used to estimate the proposed facade concept's performance within various generalized building-environment scenarios. The methodology is detailed to computationally estimate the potential environmental performance of this concept with respect to solar harvesting with adhered solar panels, as well as air changes and HVAC cost for associated interior spaces. The example scenarios include various building components, from a single room to multiple building stories, and two geographic locations with significantly different environmental conditions, and both daily and yearly performance estimates are shown. The component is most effective when the outdoor temperature is near to the desired indoor temperature and wind speeds are mild, but can still reduce HVAC usage for more disparate temperatures. For example, in the scenarios shown the component can eliminate HVAC use for a 5 °C difference between outdoor and indoor temperature and reduces HVAC usage for temperature differences up to 15 °C. Moreover, the component has the potential to significantly increase net energy generation, with yearly performance estimated for the scenarios to be as much as 25% greater than that of a flat closed façade. However, the component cut parameters can have a significant impact on environmental performance, and thus require careful design consideration.

Keywords: Kirigami-inspired façade, Environmental performance, Natural Ventilation, Solar irradiance, Real-scale Scenarios, Energy cost, Energy generation

1. Introduction

Building operations account for approximately 40% of total worldwide energy usage [1]. As a result, significant research has focused on reducing this major societal expense. Approaches to improve energy efficiency within a building's interior operation range from improving specific components, such as smart lighting [2, 3] and smart climate control [4, 5] to more comprehensive energy systems, such as smart building energy management systems [6, 7]. Alternatively, façade systems have long been designed to utilize the building exterior to contribute to the comfort of building occupants and improve building energy efficiency, with the objective of creating passive systems to control interior lighting and aid the cooling and heating of the building interior [8, 9]. Work to improve passive façade function has included increasing the efficiency of windows and window frames to decrease energy consump-

*Corresponding author
Email address: raa177@pitt.edu (Rodrigo Arauz)

tion [10, 11, 12], retrofitting existing traditional cavity walls into ventilated cavity walls to improve cooling efficiency [13] and modifying double skin façade designs [14, 15]. Additionally, there have been efforts to design the entirety of a façade's shape/orientation to reduce the amount of irradiation on a building and/or produce energy with adhered solar panels [16].

1.1. Adaptive Façade Concepts

Research has expanded beyond passive concepts to environmentally responsive façade systems [17] that adaptively change their state based upon the conditions of the surrounding environment and desired internal conditions to further improve building efficiency. There is a wide range of research exploring concepts for adaptive building façades to contribute to a diverse set of non-structural functions, including occupant thermal comfort [18, 19], energy performance [20, 21, 22], indoor air quality [23], interior acoustic performance [24, 25], visual performance [26, 23], and others [21, 27, 28, 29]. Examples of adaptive façades in-use include the Al Bahr towers [30], which is one of the most referenced adaptive façade examples and uses a Mashrabiya-inspired design for the façade. This adaptive façade uses meteorological data and sensor measurements to automatically adjust the façade panels to achieve adaptive shading for visual and thermal comfort. The SDU Kolding Campus building [31] uses an adaptive double skin façade that monitors light and heat levels and automatically activates shutters for adaptive shading. Differently from the previous examples, the Beijing Water Cube [32] has an adaptive façade with the objective of adjusting the insulating capability by manipulating the volume of air held within the façade system. Aside from the examples described in the previous, many more adaptive façade approaches are currently being investigated at the conceptual design and/or prototyping stages.

1.2. Adaptive Façade Performance Evaluation

Several adaptive façade concepts in development have had their potential environmental performance evaluated with numerical analyses [33, 34], in some cases corroborated with physical scale-models [35, 36, 37]. There is a range of specific environmental performance metrics that have been considered in such ways, including irradiance, illumination, ventilation, or combinations of these. Moreover, these concepts are being developed and evaluated using different strategies to model/estimate the environmental performance metrics and case studies to estimate potential impact. These case studies have commonly considered one geographical location and considered the adaptive façade to be acting on one example building or portion of a building (e.g., room) at that location.

For example, the work by Zupan et al. [38, 39, 35] proposed a deformable smart material façade component that changes shape with the objective of reducing the temperature gain from solar irradiation on a building's wall through self-shading. Several numerical case studies were used to demonstrate the potential performance of this concept. The case studies considered one geographical location during multiple summer days because the façade was designed for hot weather locations. Performance was estimated for both component and building-scale, and considered the use of the façade components on different portions of a building with varying façade orientation. The work by Jumabekova et al. [37] proposed an adaptive façade to also use solar interaction for thermal performance, but also included capabilities for adapting color to change the effects of solar insolation on the inside temperature of a room. A numerical model was developed from scale model testing, which was then used to evaluate a series of case studies. The case studies considered one geographical location during multiple winter days, and while the façade was only evaluated during winter, the authors discussed the possibility of parametrizing the façade for summer days as well. The study considered a single fixed-dimension room of a given building for each day. Another example is the work by Meloni et al. [33], which proposed an origami-based adaptive façade that redirects reflected sun rays to reduce solar irradiation on surrounding buildings in urban environments. Numerical case studies considered one geographical location during multiple summer and fall days in a hot weather location. The study considered the reduction of solar irradiance on the surfaces of 64 buildings of varying sizes surrounding the single building with the adaptive origami-based façade on all sides.

Adaptive ventilation has also been considered in several proposed façade concepts. Concepts targeting ventilation have mainly focused on reducing the energy consumption of a building by controlling the internal

temperature with natural airflow, rather than or in combination with climate control systems [40, 41, 36]. For example, the work by Hensen et al. [42] proposed a double skin façade that spans the whole building height, that changes the amount of opening at the bottom of the outer skin and the top of the inner skin to manipulate airflow, and ultimately the internal temperature of the building. Numerical case studies considered a single fixed-dimension multi-story building at one geographical location during multiple summer days. However, the authors state that the façade can also be beneficial during wintertime. Another example is the work done by Lucchino et al. [43], which proposed a double skin façade and a system of fans that would change the amount each skin could be opened and the various fan speeds to control airflow, and ultimately the internal temperature of the building. Additionally, the CO_2 levels in the building were also controlled with the airflow and a shading device was added in the cavity of the double skin façade to control natural illumination inside of the building. Numerical case studies considered one geographical location during multiple days at different times of the year with the objective to cool on some days and heat on others, depending on the external temperature. The location was chosen as a climate that includes both cold and hot days throughout the year. The studies considered a single fixed-dimension one-story building.

Although, as noted in the preceding, multiple promising examples of adaptive façade concepts have been evaluated for potential performance, minimal work has been done with concepts that have been designed/evaluated for, or in many cases, are even capable of achieving more than one environmental performance metric (e.g., simultaneous thermal, illumination, and/or ventilation performance). Moreover, while the example noted by Lucchino et al. [43] is among the few concepts seeking to target multiple different performance metrics (i.e., thermal, CO_2, and shading), like others, this concept requires a relatively more complex system of multiple components to achieve these metrics. Alternatively, previous studies [44, 45] have proposed the potential of kirigami-inspired concepts for adaptive façades. Kirigami-inspired structures are those that have strategically placed cuts so that when in-plane deformation is applied the cuts open and the material around the cuts deforms out-of-plane, potentially facilitating both adaptive ventilation and solar tracking for enhanced solar energy harvesting. However, research to-date has only considered the evaluation of the environmental performance of a single kirigami-inspired adaptive façade tile in isolation, rather than exploring performance at the scale of a building or even an individual room.

1.3. Problem Statement and Objectives

The current study extends the prior work [44] to evaluate the use of kirigami-inspired components for adaptive façades to be capable of considering solar harvesting and natural ventilation simultaneously. To carry out the performance evaluation of the proposed kirigami-inspired façade concept, a computational approach was established which evaluates the performance of a double skin façade with kirigami-inspired components integrated into the outer skin of the building. Additionally, to evaluate the performance comprehensively, multiple scenarios and scales were considered, including different geographical locations/climates, room sizes, and complete building performance estimation. Furthermore, different numbers of occupants and various equipment that generates heat were considered. As such, this study establishes a computational approach which is applied to evaluate the feasibility of utilizing kirigami-inspired components on a building for simultaneous control of solar interaction and natural ventilation at a range of scales and environmental conditions. The following section provides a detailed explanation of the kirigami-inspired double skin façade concept. Section 3 presents the approach used to quantify the environmental performance of the façade component in terms of mechanical behavior, ventilation, and solar harvesting. Section 4 assesses the performance of the façade component with respect to changes to design parameters and environmental conditions, as well as maximizing daily and yearly performance with respect to the total net energy generated for two building case studies.

2. Kirigami-Inspired Double Skin Façade Concept

Kirigami-inspired structures are generally defined as those that have strategically placed cuts/openings. They are a particularly promising design concept for adaptive façades due to the potential for a simple design, in terms of both manufacturing

and material selection, to provide relatively complex behavior that is beneficial in façade applications. The concept proposed herein for a kirigami-inspired façade that adaptively interacts with the sun and controls airflow into a building is based on a standard double skin design [46]. Figure 1 shows a schematic of an example of the proposed double skin façade section. Note that an entire building surface would be expected to have several sections, and even an individual room may have multiple sections depending on the size and desired level of control. However, with regards to the ventilation performance, each section is envisioned to be isolated. As such, the outer edges of each section are assumed to be impermeable to prevent air flow between two skins through the sides, top, and bottom of the section. These impermeable regions would also likely be the best candidate for connecting the components of the double skin to the building surface.

As shown in Figure 1, the inner skin of the façade section has an impermeable wall and an adjustable opening. One option could be to use an adjustable opening, and it is assumed that this would allow for controlling the amount of open area in the inner skin for ventilation. This adjustable opening could theoretically be placed anywhere on the inner skin, but its position was taken to be at the top of the inner skin for the analyses herein.

The outer skin of the section is the key feature that incorporates the proposed kirigami-inspired design. Figure 2 provides a schematic that isolates the outer skin of the façade concept and its operation to control ventilation and/or facilitate solar tracking. A cut region of the kirigami-inspired component uses the same design as presented in [44] of offset rows of straight cuts in the material. Although not generally a requirement, for the investigation presented herein, the kirigami-inspired component would be aligned such that the cuts are oriented horizontally. The bottom edge of the cut region is fixed (i.e., unmovable) to the impermeable outer edge and the upper edge of the cut region is actuated in the vertical direction to control the device. There could be multiple methods of applying this actuation, but the component was envisioned to have the upper edge of the cut region attached to a rigid window panel that can be raised and lowered by the desired actuation distance. This moving panel would slide in front of or behind the fixed window without creating any additional air gaps beyond those created by the opening cuts. Additionally, it is assumed that a flexible, but impermeable membrane is connected to the vertical edges, so that air only passes through the cut openings, rather than around the component itself.

While such details are not directly addressed in this computational study, the proposed modularized component would be expected to include a surrounding frame. This frame would include structural support to attach the double skin façade component to a building's framework. Additionally, the frame could house the mechanical system to actuate the cut region of the component, and the electrical components to supply the actuation system and transfer harvested solar energy to inverter and storage systems.

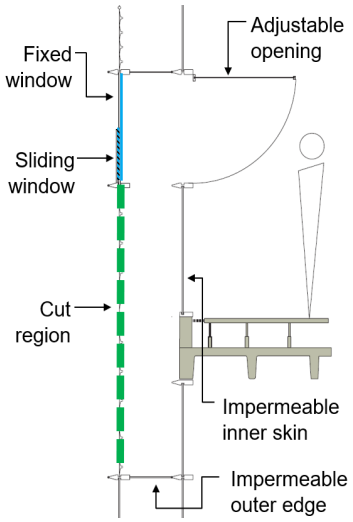

Figure 1: Side view schematic of the proposed double-skin façade concept, showing the 3 component of the outer skin, including the kirigami-inspired cut region, the sliding window to actuate the cut region, and the fixed window, the impermeable and adjustable opening components of the inner skin, and the impermeable outer edge that separates vertically adjacent façade sections.

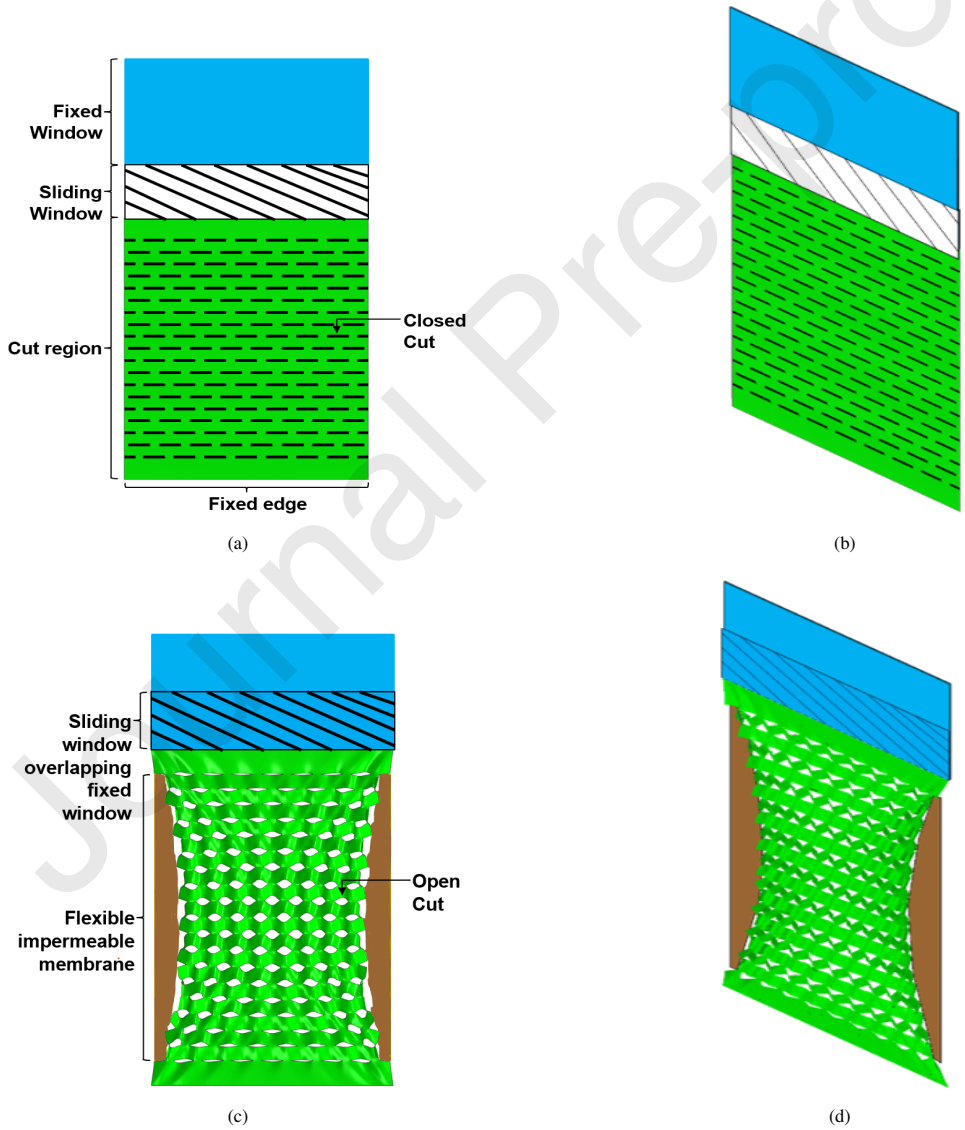

Figure 2: Front view and isometric view schematics of the extreme operational states of the outer skin of the proposed double-skin façade concept showing (a & b) the unactuated/closed cut and (c & d) maximally actuated/open cut configurations.

3. Façade Performance Evaluation Methodology

As previously noted, the objective of the present study is to numerically evaluate the potential building performance of the proposed kirigami-inspired double skin facade component considering multiple building scenarios. The computational methodology used to evaluate this performance involves a two-step analysis of the structural mechanics of the component and the environmental responses with regards to air ventilation and interaction with the sun. The two steps are as follows:

1. Structural Mechanics - Mechanical analysis estimates the deformed shape of the component given a specified actuation amount, and is used to ensure the component is sufficiently stiff and will remain undamaged throughout the actuation process.
2. Environmental Responses - The deformed shape of the component is then used together with given environmental conditions to:
    - Estimate the ventilation through the façade and into the building space to obtain the volume of airflow and impact to the climate control system (as variation in required HVAC usage) due to the convective heat transfer.
    - Evaluate the solar energy harvested as the amount of energy generated over the specified duration through solar panels adhered to the kirigami-inspired component.

The following provides the details of each performance evaluation step.

3.1. Mechanical Behavior

The same simulation method as was presented and validated in prior work [44] was applied to estimate the kirigami-inspired component geometry and external work (i.e., energy cost) for given component dimensions, cut pattern, and material properties. In brief, finite element analysis was used to evaluate the structural response of the kirigami-inspired component at any given stretch amount. Due to the relatively low thickness compared to the in-plane dimensions, the façade component was modeled as a structural shell. It was also assumed that the dynamic effects of the response would be negligible, and therefore quasi-static conditions were assumed. However, the deformation was estimated for the shell finite element model using nonlinear implicit dynamic analysis due to the relatively stable solution procedure in contrast to static or explicit analysis, and the rate of the loading was ensured to be sufficiently low to approximate quasi-static behavior. The cuts were included in the geometry as zero thickness cracks and contact between the crack surfaces was not considered as none occurred due to the chosen use case for the component. To initiate the elastic instability that produces the out-of-plane rotation of the material around the cuts, an elastic eigenvalue analysis was performed and used to perturb the initial geometry, by applying the eigenvalues as a linear superposition, prior to the analysis with the applied loading. Standard convergence tests were used to ensure that the mesh size was sufficiently small to achieve an accurate simulation for all design cases considered.

The fixed bottom of the component was assumed to have zero displacement in all directions, while the actuated top edge was assumed to have a uniform applied longitudinal displacement (i.e., the actuation amount) and all other displacement components were zero. All other boundaries of the component were assumed to be traction free. Thus, to estimate the energy cost of the actuation of each kirigami-inspired component, the total work was calculated for the actuated edge of the component. Additionally, for evaluating design admissibility, the total weight of the component (i.e. both material and solar panels) was applied as a body force and a wind load was applied as a traction to the outward facing side of the component in the direction transverse to the plane of the façade (more details on the magnitudes of the wind loads are discussed in Section 4.1). Designs, including actuation amount, were considered admissible for subsequent performance evaluation if the component was sufficiently stiff and the material remained undamaged. The stiffness was quantified by the amount the component deflects in the transverse direction when subjected to the wind load and was considered sufficient if the component deflected less than 0.5% of the component's original length. The material was assumed to remain undamaged if the Von Mises stress throughout the component did not exceed its yielding point throughout the actuation process.

3.2. Ventilation

3.2.1. Air Changes

The number of air changes can be used to quantify the amount of ventilation a closed space gains due to the airflow allowed by a façade. An air change is defined as the condition for which the air inside of a closed space is completely replaced by new air coming from the outside. Similar to the work in [47], for simplicity in the present study, the outflow was assumed to be equal to the inflow for the space considered. As such, the number of air changes over a period of time can be determined from the airflow as:

$$A_C = \frac{G_e \Delta t}{A_v} \tag{1}$$

where G_e is the estimated volume flow rate of air over a period of time, Δt is the period of time, and A_v is the total volume of air in the specified room.

To estimate the volume flow rate of air that passes through the double skin façade, the analytical model proposed by Silva et al. [48] was used. This model uses a variant of the hydrostatic equation and the Boussinesq approximation. Additionally, this model assumes that the internal and external temperature distributions are both homogeneous within the region of the façade considered and accounts for the inner and outer openings having different elevations. This analytical model was validated for estimating the airflow into a single story with an experimental scale-model. With this approach, the volume flow rate of air is estimated as:

$$G_e = \pm C_d A_r \sqrt{\left| \frac{g T_o (T_o - T_i) H}{T_i^2} \right| + V^2 \Delta C_p}, \tag{2}$$

where $\pm$ corresponds for inflow and outflow respectively, g is the acceleration due to gravity, T_o and T_i are the outdoor and indoor temperatures, respectively, H is the vertical distance between the upper and lower openings in the double skin façade, V is the wind speed, ΔC_p is the wind pressure coefficient difference between the upper and lower openings, C_d is the discharge coefficient, which is defined as the ratio between the obtained and ideal flow rate. A_r is the area coefficient between the open area of the outer skin (A_o), which is simplified to a single combined open area with its center located at the center of the kirigami-inspired component, and the open area of the inner skin (A_i), defined as:

$$A_r = \frac{2 A_i^2 A_o^2}{A_i^2 + A_o^2}. \tag{3}$$

The volume flow rate of air in Equation 2 is positive (defined as inward in this work) when the inside pressure is less than the outside pressure. This is assumed to be the case in all analysis herein.

Overall, it should be noted that while this analytical model to estimate the rate of airflow is considered sufficient for the concept evaluation here, further future refinement of this or similar façade concepts should likely include more detailed analysis of potential airflow and overall aerodynamics, such as the use of computational fluid dynamics [49, 50, 51].

3.2.2. Climate Control Impact

The temperature change in a given space due to the airflow from the natural ventilation, human presence and heat-generating equipment housed and the climate control system was quantified by assuming that heat transfer in the indoor air occurs only via conduction and that the total volume of the indoor air changes temperature at the same time. As such, the change in indoor temperature of a given space over a period of time (Δt) can be estimated as:

$$T_i(t + \Delta t) = T_i(t) + \frac{\epsilon}{(A_m S_h)} \Delta t, \tag{4}$$

where A_m is the total mass of the air in the room, S_h is the specific heat of the air and ϵ is the total of energy generated or lost in the room, with:

$$\epsilon = \epsilon_{ic} + \epsilon_h + \epsilon_v + \epsilon_{ec} + \epsilon_s, \tag{5}$$

where ϵ_{ic} is the energy provided by the internal conduction caused by the people and equipment in the room, ϵ_h is the energy provided by the climate control (i.e., HVAC) system, ϵ_v is the energy provided by the natural ventilation, which depends on the airflow:

$$\epsilon_v = G_e Q_c (T_o - T_i), \tag{6}$$

where Q_c is a heat transfer constant of the air. In addition to the convective heat transfer due to the external environment, heat conduction was also considered

through the sealed windows and walls through:

$$\epsilon_{ec} = (T_o - T_i)(U_w A_w + U_{sw} A_{sw}), \quad (7)$$

where U_w is the thermal transmittance of the walls, A_w is the total area of the walls, U_{sw} is the thermal transmittance of the sealed windows, A_{sw} is the total area of the sealed windows. Windows are also assumed to allow for energy provided by solar irradiance as:

$$\epsilon_s = A_{sw} S_{HGF}, \quad (8)$$

where S_{HGF} is the solar heat gain factor of the sealed windows.

This study assumes that there is an HVAC system dedicated to the space being considered and the assumed operation is based upon a mini-split system. Therefore, the HVAC system operates by turning on when the indoor temperature is higher or lower than a defined temperature threshold. When on, the HVAC system provides heating or cooling to the room depending on the difference between the current temperature and the desired temperature. When the indoor temperature reaches the desired temperature the HVAC will turn off, allowing the room to heat up or cool down until the threshold is reached again, repeating the cycle.

3.3. Solar Harvesting

The proposed kirigami-inspired façade concept opens up various possibilities to integrate solar harvesting devices. For example, discrete rigid lightweight solar panels could be mounted along the transverse direction of the kirigami component between each row of cuts, similarly to the work shown in [52]. Another possibility would be to bond deformable solar panels to the surface of the component, as shown in [53]. Herein, it was assumed that one of these mechanisms could be used to adhere solar panels to the kirigami-inspired component surface and the rate of energy harvested at any point on this surface is proportional to the solar irradiance at that point based on an assumed harvester efficiency.

The same method as presented in prior work [44] was applied to estimate the solar irradiance on the area covered by solar harvesters as they are moved by the kirigami-inspired component. In brief, the solar irradiance was quantified by utilizing the Hay, Davies, Klucher, and Reindl (HDKR) [54] model, which accounts for the direct beam radiation, the diffuse radiation, and the ground-reflected radiation. In this study, no external obstructions are considered, and self-shading is assumed to be negligible because the kirigami panels are small and experience relatively small rotation. Additionally, within the HDKR model, the effects of longitudinal location and altitude of the object were assumed to be negligible, and so only the latitude is necessary to define the location of the component. The total energy harvested by the component was then estimated by numerically integrating over the surface.

4. Results and Discussion

To quantify the potential environmental performance of the proposed kirigami-inspired facade concept, a fixed-size component was conceptualized and it was assumed that one or more of these components could be affixed to the external skin of a building façade, as described in the previous Section. Figure 3, shows the dimensions of the cut region of the component and the cut design parameters considered. The cut region was chosen to have planar dimensions of $2.4\ m \times 2.0\ m$, a distance between the cuts and the top and bottom boundaries of $0.2\ m$, and a thickness of $0.2\ mm$. The maximum actuation of the cut region (i.e., maximum amount the moving window section could be raised) was taken to be $0.4\ m$. The height of the sliding window section was correspondingly taken to be $0.4\ m$ so that the maximum actuation would still maintain a clear view through the fixed window. The height of the fixed window was $0.8\ m$. The adjustable opening on the inner skin was chosen to have planar dimensions of $0.8\ m \times 2.0\ m$. For all analyses, the adjustable opening was assumed to be fixed at its maximum open area at all times to examine the potential to control the ventilation with the kirigami-inspired component alone.

Although the component is evaluated computationally in this study, the material properties chosen were based on experimental work in [53]. This work used a polyimide plastic for the cut region of the component, which was similarly motivated by the objective of solar tracking and performed experiments with solar panels attached to the surfaces around the cuts. Thus, the material of the cut region of the component was as-

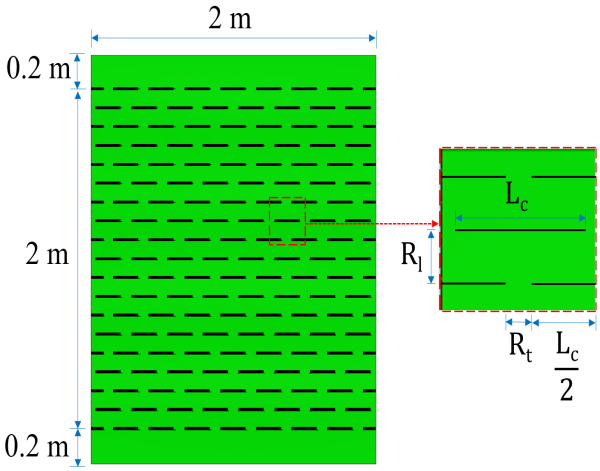

Figure 3: Dimensions of the cut region of the example double-skin façade concept considered and a zoomed-in view showing the cut design parameters of a unit cell of the kirigami-inspired design.

sumed to be isotropic, homogeneous, and linear elastic, with a Young's modulus of 2.5 GPa, a Poisson's ratio of 0.34, and a density of 1420 $\frac{kg}{m^3}$, based on typical values for polyimide plastic [55]. The solar panels were assumed to be semi-flexible, and capable of withstanding wind speeds higher than 20 $\frac{m}{s}$ at 10 meters in height [56], with an efficiency of 15 %. The polyimide material was chosen since it has been previously shown experimentally to function as desired with the chosen straight cut pattern, but formal selection of materials and additional solar panel details is left for future work.

To evaluate the structural constraint (i.e., whether the component is deflecting in the transverse direction more than 0.01 m.), a body force was applied to the component accounting for the self-weight of the polyimide plastic and the weight of the adhered solar panels, which was a total of 18, 100 $\frac{N}{m^3}$. Additionally, a traction of 123 Pa was applied transversely to the component, based on a wind speed of 10$\frac{m}{s}$ when the component is assumed to be at 10 meters in height, which is the maximum wind speed considered for the following test cases.

For the ventilation, the discharge coefficient (C_d) of the openings in the outer skin was assumed to be 0.44, based on tests presented in [57, 58] for elliptic openings, which are similar in shape to the openings in the proposed component. The opening in the inner skin was assumed to have a discharge coefficient of 0.8, which is the maximum value identified in [59] for an open area (i.e., the adjustable opening in the inner skin was assumed to be opened to its maximum extent). For the heat transfer between the outside and the inside, the thermal transmittance (U-value) of the walls was 2.0 $\frac{W}{m^2K}$ to approximate solid brick walls. The U-value for the windows depends on the location, which varies for the following test cases and is provided in the relevant subsections.

For all test cases, the initial temperature of the indoor space was assumed to be 22.0 $°C$. Additionally, the HVAC system was assumed to be off at the starting time and programmed to turn on when the indoor temperature falls below 20.0 $°C$ or above 24.0 $°C$, based on the recommendation of the Occupational Safety and Health Administration for office spaces [60]. When activated, the HVAC system remains on until the indoor temperature reaches 22.0 $°C$. The capacity of the HVAC systems considered, and therefore, their efficiency was defined based on the size of the space considered assuming conditions with no natural ventilation, with these details provided in the following subsections. The heat generated from miscellaneous equipment and the number of people within the space also depended on the specific space considered, while each person was assumed to generate 112 $\frac{W}{h}$ of heat [61].

The component performance was evaluated for all combinations of a test matrix of the three cut design parameters, yielding 48 total potential designs for the kirigami-inspired component:

- The ratio of the distance between the cuts (i.e., cut spacing) and the length of the cuts in the direction transverse to the actuation direction ($R_t : L_c$), with three different cases: 1 : 2, 1 : 4, and 1 : 8.
- The number of cells in the transverse direction (N_t), with four different cases: 10, 15, 20, and 25.
- The number of cells in the direction parallel to the actuation direction (N_l), with four different cases: 10, 15, 20, and 25.

The first set of tests in the following subsection were used to identify the environmental conditions, in terms of outdoor air temperature and wind speed, for which the kirigami-inspired component could potentially reduce the HVAC usage, and thus, the energy cost for temperature control. Temperature control was considered alone first since it is the only objective that could potentially increase the energy cost of the building if

the component is used ineffectively. Additionally, temperature control is often the most (or one of the most) energy expensive aspects of building operation. Therefore, these first tests provide guidance as to what environments (i.e., locations and time periods) may benefit most from the proposed façade concept and helped guide the subsequent more specific case studies considered to evaluate potential building performance impacts. The subsequent case studies then considered the component adhered to varying portions of a building in two locations that have significantly different environmental conditions, to evaluate potential contributions to a building's environmental performance in terms of HVAC use, air changes, and solar energy generation.

4.1. Performance on an Arbitrary Location with Varying Environmental Conditions

For the initial tests, the component was considered as an isolated element in an arbitrary location as the façade of a single room. The size of the room was chosen to be $2.0\ m \times 6.0\ m \times 3.5\ m$. The room had single glazed windows with a U-value of 5.2 $\frac{W}{K \cdot m^2}$ and a solar heat gain factor of 0.525. The air leakage rating for the windows was 1.23 $\frac{m^3}{h}$, and the air leakage rating was arbitrarily assumed to be 0.492 $\frac{m^3}{h}$ for the kirigami-inspired component per unit of windspeed. Six people were assumed to be within the room for the entire evaluation period and an additional 1100 $\frac{W}{h}$ of heat was assumed to be generated by miscellaneous equipment inside the room, such as computers and lighting. Based on these specifications, the HVAC system for the room was required to have a capacity of 1 ton. These specifications were chosen such that the room would gradually increase in temperature if the kirigami-inspired component was completely closed and no HVAC was used. Therefore, the outdoor temperature would need to be lower than the desired indoor temperature for there to be any potential benefit in employing the component to reduce the need for HVAC to cool the indoor space. As such, four outdoor temperatures were considered: $-5.0, 0.0, 10.0$, and $15.0\ ^\circ C$. Additionally, four wind speeds were considered for each outdoor temperature, all within the range of gentle breeze on the Beufort scale : $1.0, 1.5, 2.0$, and $3.0\ \frac{m}{s}$ measured at 10 meters.

The total time to evaluate the HVAC performance was four hours from 12:00 to 16:00. Additionally, since only the total size of the openings (i.e., open area) created in the kirigami-inspired component during operation affects the indoor temperature, and therefore HVAC operation, the evaluation of the potential cut designs was simplified to the range of open area of all designs, which ranged from zero (no actuation/closed component) to the maximum amount of open area for the 48 design cases considered of 1.31 m^2, which is obtained from the numerical simulations.

Figure 4 shows the required operation of the HVAC with respect to the amount of open area of the kirigami-inspired component held fixed for the 4-hour evaluation period for each scenario of environmental conditions. The blue and red portions indicate that the HVAC needed to cool or heat the space, respectively, for some amount of time during the period, black indicates that the HVAC never needed to be activated during the 4-hour period, and the hatched portion indicates that the amount of HVAC operation time needed was greater than the control condition of the component being closed.

For the majority of the scenarios considered, the kirigami-inspired component provides some benefit in reducing the HVAC usage required to maintain the internal temperature regardless of the amount it was opened. Additionally, there are several scenarios that can utilize the component to maintain the desired internal temperature with no HVAC usage at all. In particular, each chosen outdoor temperature has a range of component operation that requires no HVAC to maintain the desired indoor temperature range over the 4-hour evaluation period, provided with sufficient wind speed. Although it should be noted that for the scenarios where HVAC would not be required at all during the 4-hour period, the HVAC would eventually need to be used if the duration had been greater than 4 hours and conditions remained similar, as temperature within the room never remained constant. This eventual need for HVAC could potentially be eliminated however with dynamic operation of the proposed component, which could be closed or opened to decrease or increase the cooling effect, respectively.

As noted, based on the room conditions, the benefit of the kirigami-inspired component is to reduce the need of the HVAC to cool the room, and thus, had the outdoor temperature been closer to the desired indoor temperature range the benefit of the component would be reduced. If the outdoor temperature exceeded the de-

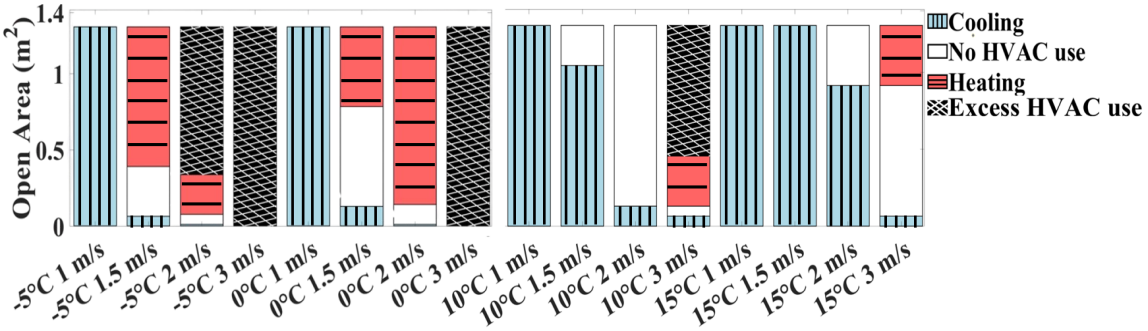

Figure 4: HVAC requirements for a single room at an arbitrary location with the kirigami-inspired component attached to the façade fixed for 4 hours at the specified amount of open area of the outer skin cut region (vertical axis) with the specified outdoor temperature and wind speed, indicating whether the indoor temperature can be maintained with no HVAC use (no color), less HVAC use than a corresponding closed facade system to either cool (blue with vertical lines) or heat (red with horizontal lines) the room, or more HVAC use than the corresponding closed facade system to heat the room (black with cross hatching).

sired indoor temperature range, there would be no benefit to utilizing the component to reduce HVAC cost. As is evident in the results presented, the opposite extreme of low outdoor temperatures and high wind speeds also eliminates the benefit of the component to reduce the HVAC cost. However, for higher temperatures that are still at or below the desired indoor temperature, having higher wind speed than those considered here would be expected to improve the effectiveness of component in most cases. Generally, there may still be a benefit in nearly any environmental condition to increase air changes (i.e., ventilation) or improve solar interaction (i.e., solar harvesting), depending on the importance given to these sometimes competing objectives.

Summarizing the observations of these initial tests, there is a relatively wide range of environmental conditions for which the kirigami-inspired component can reduce the energy required for an HVAC system to maintain a desired indoor temperature of an occupied space. The component is particularly effective in terms of HVAC usage when the outside temperature is lower than the indoor temperature, but relatively close to the desired indoor temperature and the wind speed is significant (e.g., 10 $^{\circ}C$ with 2 $\frac{m}{s}$ or 15 $^{\circ}C$ with 3 $\frac{m}{s}$ for the cases considered here). Due to these observations, two case studies were selected based on typical environmental conditions to further evaluate the potential performance of the proposed kirigami-inspired component, one in which the proposed component could potentially benefit HVAC cost relatively consistently through an entire year - San Diego, California, USA, and the other in which benefits to HVAC usage are only possible for a portion of the year - Pittsburgh, Pennsylvania, USA.

4.2. *Building Performance Case Studies*

As noted, two locations were considered: San Diego, California, USA with a latitude of 32.7° and Pittsburgh, Pennsylvania, USA with a latitude of 40.0°. San Diego was chosen because the temperature is relatively constant throughout the year, with the yearly average temperatures having a standard deviation of 2.8°C. Alternatively, Pittsburgh was chosen because of the significant changes in temperature throughout the year, with the yearly average temperatures having a standard deviation of 9.0°C.

For each of the two defined locations, two different situations were considered. As shown in Figure 5a, first the effects on a single space on the second story of an office building (i.e., first floor above the lobby) at a floor elevation of 4.5 m was evaluated. Second, as shown in Figure 5b, the total effects of the same space repeated on 6 identical stories of a 7-story building starting from the second story was evaluated. For all considered cases, both the temperature and the wind speed given were assumed to be the ground level. The temperature was assumed to vary linearly with elevation at 0.1°C every 10 meters according to the dry adiabatic rate [62]. The wind speed was assumed to be 3 $\frac{m}{s}$ at ground level and was assumed to change exponentially with elevation based on the wind shear [63]. The characteristics of the space considered were the same for every floor analyzed. The floor-plan is representative of a meeting room with a floor area of 12.0 m^2 and ceiling height of 3.5 m, and with a single kirigami-inspired component attached to one southwest-facing exterior wall. Similarly to the initial tests, the meeting room was assumed to be occupied at all times by six peo-

(a) (b)

Figure 5: Schematics showing the vertical dimensions and adaptive façade component locations for the (a) single-story building scenario and (b) multi-story building scenario considered for the building case studies.

ple and 1100 $\frac{W}{h}$ of heat was assumed to be generated by miscellaneous equipment inside the room. Based on these specifications, the HVAC system for the room was required to have a capacity of 1 ton with an overall efficiency rating of 13. The kirigami-inspired components were assumed to be able to be operated independently for each story. Additionally, the actuation for each component was assumed to be able to be prescribed once per hour, at the start of the hour, the actuation could be applied in increments of 2 *cm* from the 0 (i.e., no actuation) to the maximum actuation of 40 *cm* considered, and the time necessary to complete the actuation process was assumed to be negligible.

To evaluate the potential performance at each location, first a single day was considered, referred to as the "base design date", which was evaluated for a period of 4 hours, from 8:00 to 12:00. This base design date was chosen to be representative of a relatively large portion of the year, such that it experienced moderate solar exposure and relatively large, but not extreme temperature variation for the location. More specifically, the base design date was chosen to be no more than ±7 days from either the vernal or autumn equinox and had a minimum and maximum temperature over the 8-hour period nearest to $5°C$ and $20°C$, respectively. Note that the temperature range was chosen to be limited to the range for which the proposed component was determined to be potentially beneficial from the analysis in Section 4.1.

The base design date identified was used to evaluate the variations in the component design, including cut number/dimensions and the actuation sequence, that would be preferable depending on the variations in the objectives for air changes, energy generation, and/or energy usage. Initially, to evaluate the spectrum of design options that could potentially maximize air changes with minimal HVAC usage, the subset of the 48 potential cut designs was identified that could achieve the range of open area within the component to maximize total air changes over the 8-hour period for the base design date as:

$$\begin{aligned} &\max_{\vec{\alpha}} \quad \sum_{i=1}^{8} A_i \\ &\text{s.t.} \quad 2.1 \leq A_i \leq 18, \ \forall i, \text{and} \\ &HVAC = 0, \text{with } 20^\circ \leq T_{Ii} \leq 24^\circ, \ \forall i \end{aligned} \tag{9}$$

where $\vec{\alpha}$ is the sequence of component open areas for each hour, constrained such that the hourly air changes, A_i, are within the ASHRAE recommended minimum and maximum for 6 occupants of 2.1 and 18 [64], and the hourly internal temperature, T_{Ii}, is within the previous defined limits without any HVAC usage. Therefore, the subset (D_c) of the set of 48 component cut designs (D) can be defined based on this objects as:

$$D_c = \{\vec{c} \in D : \alpha_{max}(\vec{c}) \geq \|\vec{\alpha}\|_\infty\}, \tag{10}$$

where $\vec{c}$ is the set of cut design parameters, α_{max} is the maximum open area achievable for the design within the predefined actuation limit, and $\|\cdot\|_\infty$ is the standard l_∞-norm. Three specific sets of cut designs from the subset and their associated actuation sequence were then identified based upon three different energy objectives, while still maintaining no HVAC usage and sufficient air changes: (1) maximizing the solar energy harvested, (2) minimizing the energy cost (in this case, work from actuation), and (3) maximizing the net energy generated. These three energy-based objectives can be written, respectively, as:

$$\max_{\vec{c}\in D_c,\vec{s}} \quad \sum_{i=1}^{8} E_{g_i} \tag{11a}$$

OR

$$\min_{\vec{c}\in D_c,\vec{s}} \quad \sum_{i=1}^{8} E_{ci} \tag{11b}$$

OR

$$\max_{\vec{c}\in D_c,\vec{s}} \quad \sum_{i=1}^{8} \left(E_{g_i} - E_{ci}\right) \tag{11c}$$

$$\text{s.t.} \quad 2.1 \le A_i \le 18, \ \forall i, \text{and}$$
$$HVAC = 0, \text{with } 20^\circ \le T_{Ii} \le 24^\circ, \ \forall i$$

where $\vec{s}$ is the set of hourly actuations (i.e, the actuation sequence) and E_{g_i} and E_{ci} are the hourly energy harvested and energy cost, respectively. For comparison, the cut design and associated actuation sequence from the entire set of 48 cut designs (i.e., including designs that may require HVAC usage and/or may not be able to maximize air changes) that maximizes the net energy generated was identified as:

$$\begin{aligned} &\max_{\vec{c}\in D,\vec{s}} \quad \sum_{i=1}^{8} \left(E_{g_i} - E_{ci}\right) \\ &\text{s.t.} \quad 2.1 \le A_i \le 18, \ \forall i, \text{and} \\ &20^\circ \le T_{Ii} \le 24^\circ, \ \forall i \end{aligned} \tag{12}$$

noting that the energy cost (E_{ci}) may now include the HVAC energy cost as well as the actuation energy cost.

Lastly, the component design (i.e., cut number/dimensions) that provided the maximum net energy generation with no HVAC usage for the base design date (Equation 11c) was used to estimate the potential performance of the proposed component over an entire year. It was again necessary to identify representative days for the environmental conditions of the location over a year. As such, a set of days was identified with an iterative process to find the minimum number of days that can be assumed to represent the variations in temperature and solar position throughout a year. First, the year was divided into the 4 seasons, and 1 representative day per season was selected. A day was considered representative of a period of time if that day has minimum temperature no more than 4 degrees greater than the minimum seasonal temperature and a maximum temperature no more than 4 degrees less than the maximum seasonal temperature during the defined 8-hour period. If a day satisfying the criteria could not be identified, then the period of time was divided approximately in half, and the process to identify a representative day was repeated. This iterative procedure was performed until a set of days representative of the entire year was identified. For each day in the set, the actuation sequence for the component with the pre-determined cut design was identified to maximize the total net energy for the 8-hour period as:

$$\begin{aligned} &\max_{\vec{s}} \quad \sum_{i=1}^{8} \left(E_{g_i} - E_{ci}\right) \\ &\text{s.t.} \quad 20^\circ \le T_{Ii} \le 24^\circ, \ \forall i \end{aligned} \tag{13}$$

In this case, the constraint on the number of air changes per hour (i.e., $2.1 \le A_i \le 18$) was applied as a soft constraint that only took effect if the desired temperature range could be maintained. This was necessary since some extreme temperature cases throughout a year will exceed the capability of the HVAC system if any amount of opening of the component is allowed. The annual capability of the component was therefore estimated by a weighted sum of the performances of each day considered, where the weighting for each day is the number of days in the period of the year it represented.

4.2.1. Single Story in San Diego, California, USA

Figure 6 shows the sequence of open area necessary to maximize air changes within the ASHRAE limits, while ensuring no HVAC use is required to maintain the desired internal temperature (Equation 9) for the base design date of March 25, 2023. Only two actuations (i.e., open area changes) are needed, one to start the day at 8:00 and a second at 11:00, with that second

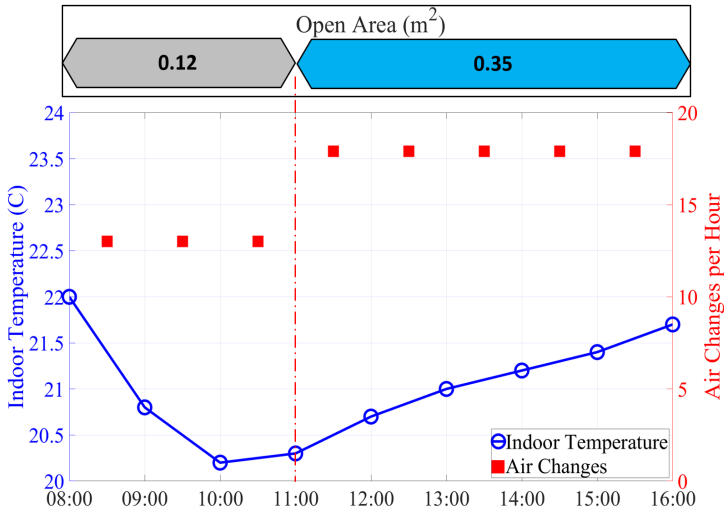

Figure 6: Indoor temperature at each hour, the number of air changes for each hour (indicated at the half-hour), and the corresponding open area the component would be actuated to at each hour to maximize the number of air changes without requiring any HVAC use to maintain the desired indoor temperature for the base design date for the single story building scenario in San Diego between 8:00 and 16:00.

configuration held for the rest of the day. It is the second actuation that maximizes the air changes per hour near to the upper limit, with an open area in the component of $0.35m^2$, whereas in the morning, when the outside temperature is lower, the component needs to be maintained at a lower open area to ensure that the indoor temperature does not fall below the desired range. However, even at the lower amount of open area, the air changes per hour are still far closer to the upper bound than the lower bound, showing the potential to significantly increase indoor air quality regardless, even at lower levels of actuation.

Assuming that the component could be actuated with a high level of precision, regardless of the cut design parameters, 19 out of the 48 designs are part of the subset D_c which can achieve at least the 0.35 m^2 of open area needed to maximize air changes with no more than 0.4 m of actuation. Thus, there is a relatively large variety of cut design parameters that could achieve the maximum air changes without using the HVAC system for the scenario considered. Yet, a common characteristic of the 19 designs is that the length of the cut is significantly bigger than the distance between the cuts in the transverse direction, in other words, the ratio $R_t : L_c$ is relatively small. As shown in prior work [44], when $R_t : L_c$ is smaller, there is generally an increase in the amount of open area per unit of actuation. Therefore, designs with a low $R_t : L_c$ were more likely to be capable of at least 0.35 m^2 of open area.

Table 1 and Figure 7 show the cut parameters and the corresponding actuation sequence over the 8 hour period, respectively, for the cut designs that maximize energy harvested (Equation 11a), minimize energy cost (Equation 11b), and maximize net energy generated (Equation 11c), all with the constraint of no HVAC usage. Note that the design that maximized the net energy generated from all 48 cut parameter design options (Equation 12) was determined to be the same design (cut parameters and actuation sequence) as that which maximized the net energy with no HVAC usage (Equation 11c). Additionally, Table 2 shows the environmental performance of all three designs, including the average air changes per hour, the total energy harvested, the total actuation cost, and the net energy generated. A first note is that the same design was identified to maximize the net energy regardless of whether the constraint of no HVAC usage was applied. This is due to the base design date being chosen for its favorably mild outdoor temperature range, which allows the device to be manipulated to maximize energy harvested without the additional ventilation at higher actuation levels significantly affecting the indoor temperature. As shown in the subsequent analysis, this is not the case on days with more variable or unfavorable outdoor temperature ranges, where there is a tradeoff between HVAC usage and net energy generation. Otherwise, significantly different cut parameters and actuation sequences were identified depending on the energy-related objective.

The most significant performance difference between the component designs is the energy cost (i.e., ac-

Table 1: The cut design parameters, including the number of cells in the longitudinal direction (N_l), the number of cells in the transverse direction (N_t), and the ratio of the distance between the cuts and the length of the cuts ($R_t : L_c$), to maximize the energy harvested with no HVAC use (Max $\sum_i E_{g_i}$, $HVAC = 0$), to minimize the actuation energy with no HVAC use (Min $\sum_i E_{ci}$, $HVAC = 0$), and to maximize the net energy generated (Max $\sum_i (E_{gi} - E_{ci})$) for the base design date for a single story building scenario in San Diego (note that the colors for each objective match those used for Figure 7).

Objective	N_l	N_t	$R_t : L_c$
Max $\sum_i E_{g_i}$, $HVAC = 0$	10	25	1 : 8
Min $\sum_i E_{ci}$, $HVAC = 0$	25	10	1 : 8
Max $\sum_i (E_{gi} - E_{ci})$	15	10	1 : 8

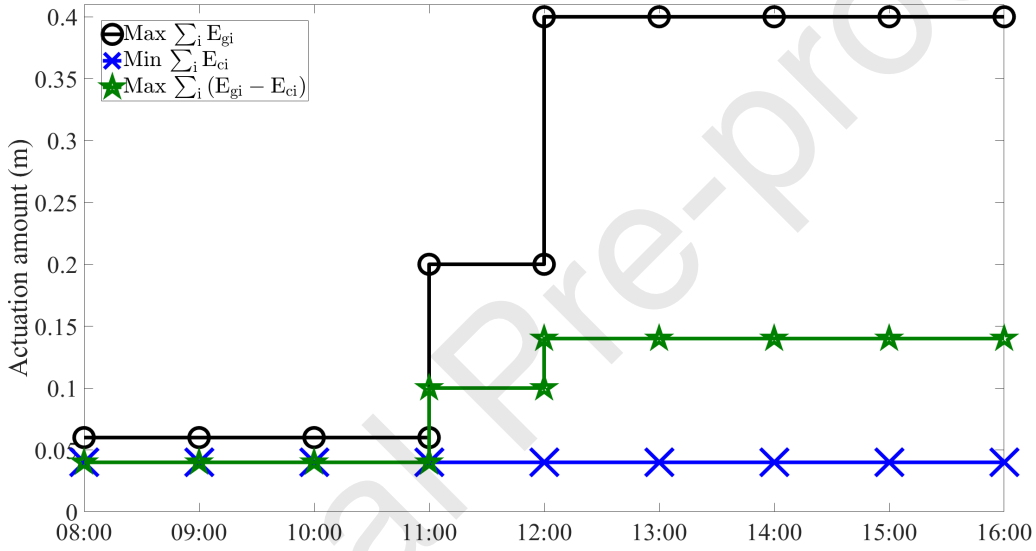

Figure 7: The amount of actuation at each hour for the kirigami-inspired component with the corresponding cut designs given in Table 1 to maximize the energy harvested with no HVAC use (Max $\sum_i E_{g_i}$, $HVAC = 0$), to minimize the actuation energy with no HVAC use (Min $\sum_i E_{ci}$, $HVAC = 0$), and to maximize the net energy generated (Max $\sum_i (E_{gi} - E_{ci})$) for the base design date for a single story building scenario in San Diego (note that the colors for each objective match those used for Table 1).

Table 2: The average air changes per hour (A_h), the total energy harvested (E_g), the total actuation cost (E_c), and the net energy generated (E_t) to maximize the energy harvested with no HVAC use (Max $\sum_i E_{g_i}$, $HVAC = 0$), to minimize the actuation energy with no HVAC use (Min $\sum_i E_{ci}$, $HVAC = 0$), and to maximize the net energy generated (Max $\sum_i (E_{gi} - E_{ci})$) for the base design date for a single story building scenario in San Diego (note that the colors for each objective match those used for Table 1).

Objective	A_h	$E_g(W)$	$E_c(W)$	$E_t(W)$
Max $\sum_i E_{g_i}$, $HVAC = 0$	14.5	4859	540	4319
Min $\sum_i E_{ci}$, $HVAC = 0$	13.4	4345	7	4333
Max $\sum_i (E_{gi} - E_{ci})$	14.6	4700	20	4680

tuation work). In particular, the cut parameters and actuation sequence that maximized solar energy harvested required more than an order of magnitude higher of actuation work than the other designs. As expected, some of the additional cost is due to the design having more changes in the actuation throughout the day to track the changing position of the sun. This design also has a higher number of cells transverse to the direction of actuation (N_t) and a lower number of cells in the direction of actuation (N_l), which leads to higher required actuation forces, but a lower amount of open area relative to the amount of rotation of the surface around the cuts where the solar panels would be attached, as show in prior work [44]. Therefore, the solar panels could be rotated more, which was preferable for the scenario considered, without increasing the air changes above the allowable limit. Yet, the relatively large increase in the energy cost only provided an approximately 8% increase in the solar energy harvested compared to the design that maximized the net energy generated. Alternatively, the energy cost of the design that maximized net energy generated is not significantly greater than the energy cost of the design that minimized the energy cost, as both designs have a low N_t and high N_l value (opposite of the $N_t - N_l$ relationship for the design that maximized solar energy harvested), which leads to lower required actuation forces in general. As such, the tracking of the sun can still be significantly improved through intelligent selection of the cut parameters and/or actuation sequence without a substantial increase in energy cost to operate the component. Moreover, all of the designs had similarly high amounts of air changes near to the maximum allowable, despite the variations in cut parameters and actuation sequences. This further emphasizes the relatively flexibility of the proposed component to improve multiple environmental performance objectives with a range of cut parameters with sufficient actuation control.

As noted, the cut parameters that were identified to maximize the net energy generated with the constraint of no HVAC usage for the base design date ($N_l = 15$, $N_t = 10$, $R_t : L_c = 1 : 8$), were applied to the set of days representative of a year, with the actuation sequence determined that maximizes the net energy generated for each day. The six days identified to represent the year 2023 in San Diego, along with the corresponding range of dates each day represents and the temperature at the start, midpoint, and end of each day are shown in Table 3.

Table 4 shows the environmental performance of the six representative days for the optimized actuation sequence, including the total air changes, the total energy harvested, the energy cost from actuation, the energy cost from HVAC use, and the total net energy generated. There is significant variation in all of the performance measures throughout the year. The energy harvested changes considerably as expected, with the highest value nearest to the summer solstice and lowest nearest to the winter solstice. Similarly, the energy cost of the HVAC increases when temperatures are more extreme, which is the higher outdoor temperatures of summer in this case. It should also be noted that all six days required HVAC usage. Although variable, the energy cost of the actuation was relatively low for each day, again due to the cut parameters leading to a lower actuation cost of the component.

The weighted sum estimate of the total net energy for the year is 1.41 MW, which is an average daily amount of 3864 W. This daily average is lower than the maximum net energy attainable on the base design date, but still a relatively large amount of energy gained. For context, a closed façade system with a continuous vertically oriented solar panel of the same type considered with a total exposed surface area equal to the unactuated component surface area would net approximately 1.13 MW over the year (3096 W on average per day). Thus, the proposed component is able to achieve a net energy gain almost 25% greater than a baseline flat and closed façade system. Other similar adaptive façade technology has been shown to improve net energy performance of buildings between 10% and 30% through combinations of solar energy harvesting, ventilation or shading when compared to standard static façades [43, 65, 66].

The proposed component also has the ventilation benefit, with the performance able to remain near to the maximum allowable air changes year-round. The weighted daily average of air changes per hour over the year was estimated as 14.2, which is only 3% lower than the maximum air changes estimated for the base design date. The air changes are able to remain high, even though they were not targeted as an objective of the optimization. The high number of air changes are possible largely due to the generally mild conditions in San

Table 3: The dates identified to represent the variation in environmental conditions throughout the year 2023 for San Diego, as well as the corresponding range of dates represented and the temperature at the start (8:00), middle (12:00), and end (16:00) of the evaluation period for each date.

Date	**Date Range**	**Temperature at 8:00** ($°C$)	**Temperature at 12:00** ($°C$)	**Temperature at 16:00** ($°C$)
January 7	12/22 to 2/4	7.8	18.9	18.3
February 16	2/5 to 3/19	5.0	17.8	15.0
March 27	3/20 to 5/5	8.9	18.9	19.4
June 20	5/6 to 6/20	17.8	21.1	22.2
August 29	6/21 to 9/22	20.6	25.6	27.8
October 31	9/23 to 12/21	10.6	25.0	25.6

Table 4: The average air changes per hour (A_h), the total energy harvested (E_g), the total actuation cost (E_c), the energy cost required to use the HVAC (HVAC), and the net energy generated (E_t) for the cut design that maximized net energy generated for the base design date and with an actuation sequence that maximized net energy generated for each representative date for the year 2023 for the single story building scenario in San Diego.

Date	A_h	$E_g(W)$	$E_c(W)$	$HVAC(W)$	$E_t(W)$
January 7, 2023	14.7	3331	18	180	3133
February 16, 2023	14.5	4070	30	113	3906
March 27, 2023	13.9	4675	21	81	4573
June 20, 2023	12.7	5394	25	716	4653
August 29, 2023	13.9	4977	21	965	3991
October 31, 2023	15.6	3727	20	428	3279

Diego year-round, but in general depend on the tradeoff between the capability/efficiency of the solar harvesting method, the HVAC system, and the environment (particularly temperature and wind speed).

4.2.2. Multi-story in San Diego, California, USA

The cut parameters that were identified to maximize the net energy generated with the constraint of no HVAC usage for the base design date with the single story scenario were used to evaluate the potential multi-story performance. In this case, the actuation sequence that maximizes the net energy generated for each day at each floor was determined (i.e., each floor was allowed to have an independent actuation sequence). Figures 8 and 9 show the resulting net energy generated and the average air changes per hour for each of the representative days at the 2nd, 4th, and 7th floors of the building.

Overall, the specific nature of the change in performance with floor height (i.e., increasing or decreasing and magnitude of the change) is relatively complex, as it depends on not just the increase of wind speed and decrease of temperature due to height, but also the overall range of temperature and positioning of the sun throughout a given day, which all affect the potential solar energy generation and HVAC energy cost. For example, the relatively warm day of June 20 results in an increased performance with height, while the hotter day of August 29 and the remaining cooler days generally have decreased performance with height. Regardless, with few exceptions the performance quantities do not change by a large amount with respect to the floor level, as the average change in the energy and air change performances from floor to floor were 101.167W and 0.663 and the standard deviations were 90.305 W and 0.511, respectively.

The weighted sum estimate of the total net energy for the entire multi-story building for the year is 7.84 MW, which is an average daily amount of 21.5 KW, and the weighted daily average of air changes per hour over the year is 13.24. Therefore, the total estimated energy performance of the building with 6 active floors is 5.56 times greater than the estimated performance of 1 active floor. The average air changes for each space is 6.77% less for the multi-story system compared to the single story. As such, there is a decreasing performance per floor for a multi-story system, but this decrease per floor is relatively small and the overall potential performance is still significant for this scenario.

4.2.3. Single Story in Pittsburgh, Pennsylvania, USA

The same base design date of March 25, 2023 was identified for Pittsburgh as was found for San Diego. Figure 10 shows the sequence of open area nec-

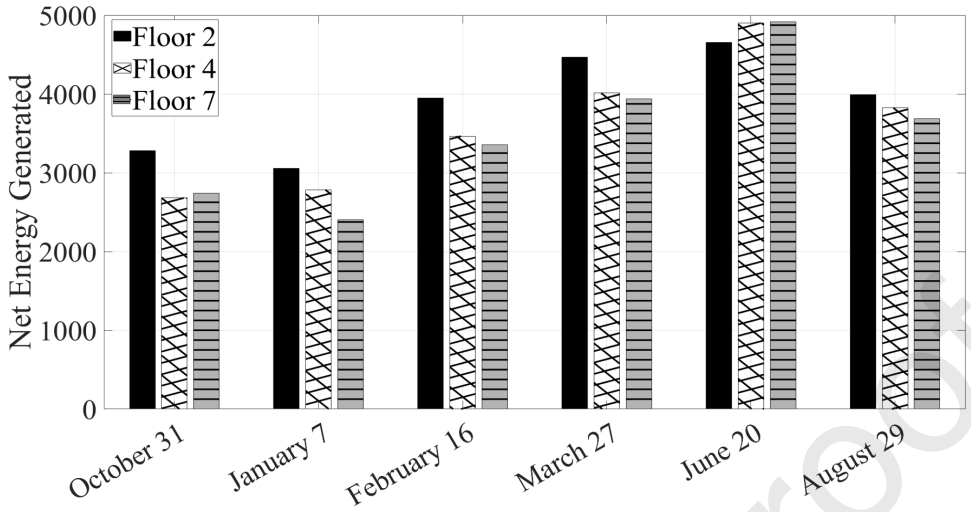

Figure 8: The net energy generated individually for floor 2 (black), floor 4 (white with cross hatching), and floor 7 (grey with horizontal lines) for the cut design that maximized net energy generated for the base design date and with an actuation sequence that maximized net energy generated for each representative date for the year 2023 for the single story building scenario in San Diego.

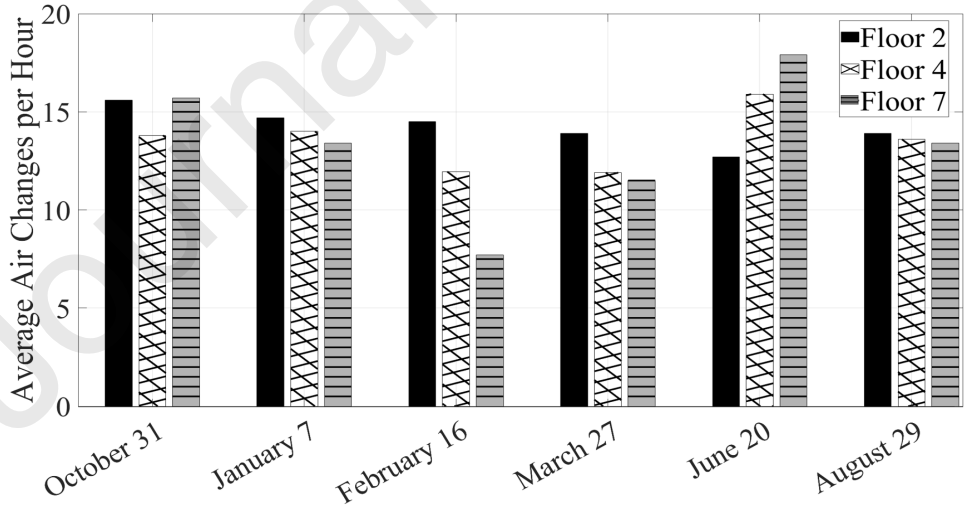

Figure 9: The average air changes per hour for floor 2 (black), floor 4 (white with cross hatching), and floor 7 (grey with horizontal lines) for the cut design that maximized net energy generated for the base design date and with an actuation sequence that maximized net energy generated for each representative date for the year 2023 for the single story building scenario in San Diego.

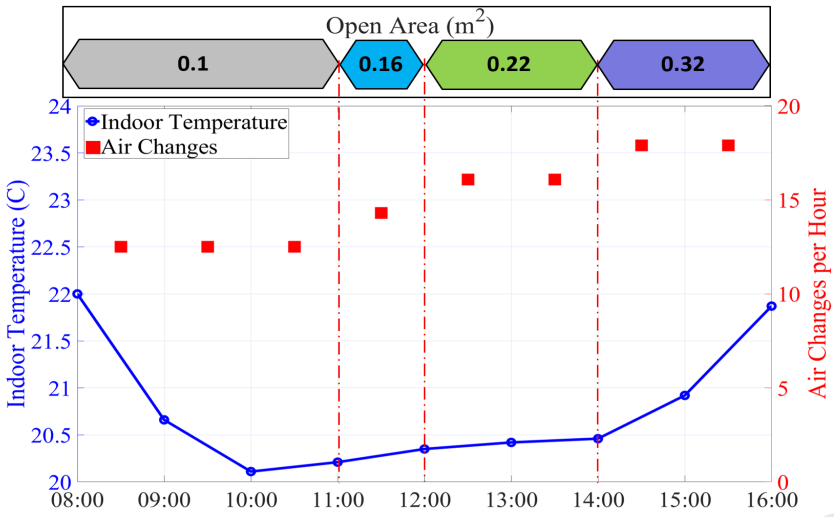

Figure 10: Indoor temperature at each hour, the number of air changes for each hour (indicated at the half-hour), and the corresponding open area the component would be actuated to at each hour to maximize the number of air changes without requiring any HVAC use to maintain the desired indoor temperature for the base design date for the single story building scenario in Pittsburgh between 8:00 and 16:00.

essary to maximize air changes within the ASHRAE limits, while ensuring no HVAC use is required to maintain the desired internal temperature (Equation 9) for the base design date in Pittsburgh. In contrast to San Diego, two more actuation changes of the component are required throughout the day, for a total of four actuation changes at 8:00, 11:00, 12:00, and 14:00. As previously, the final actuation leads to nearly the maximum open area, and thus air changes, while the colder temperatures earlier in the day require a less open façade. The maximum open area for Pittsburgh is slightly smaller than San Diego at 0.32 m^2. The slower rate of temperature increase during the day compared to San Diego results in a lower maximum actuation and there are additional intermediate actuations needed to maximize the performance. As such, the average air changes per hour is 10% lower for Pittsburgh compared to San Diego, but the air changes per hour throughout the day are still significantly higher than the minimum air changes per hour required.

Since a lower open area is needed for Pittsburgh, an even larger range of designs can achieve the maximum air changes, resulting in 21 out of the 48 designs being part of the subset D_c. However, the common characteristic of the design space remains consistent, with the ratio of the distance between cuts in the transverse direction to the cut length being relatively small for all designs included.

Table 5 and Figure 11 show the cut parameters and the corresponding actuation sequence over the 8 hour period, respectively, for the cut designs that maximize energy harvested (Equation 11a), minimize energy cost (Equation 11b), and maximize net energy generated (Equation 11c), all with the constraint of no HVAC usage. As was the case for San Diego, the design that maximized the net energy generated from all 48 cut parameter design options (Equation 12) was the same design as that which maximized the net energy with no HVAC usage. Thus, there was still no energy benefit to allow for HVAC usage. Additionally, Table 6 shows the environemntal performance for the three chosen designs, including the total number of air changes, the energy harvested, the energy cost, and the net energy generated.

Somewhat surprisingly, the same cut design parameters as found for San Diego were identified to maximize energy performance, even though the environmental conditions of Pittsburgh are significantly different. However, since the same base design date was identified and the latitudes of the locations are similar, the potential solar energy harvested for that date is similar, even though Pittsburgh has a lower solar energy harvested in all cases, due to a lower clearness index. For Pittsburgh, the same cut design parameters were also found to maximize the energy harvested, as the reduction in potential actuation reduced the solar harvesting effectiveness of the cut design parameters identified for San Diego. In general, due to the lower average temperature of the day, the amounts of opening for all cases in Pittsburgh were less than the corresponding cases in San

Table 5: The cut design parameters, including the number of cells in the longitudinal direction (N_l), the number of cells in the transverse direction (N_t), and the ratio of the distance between the cuts and the length of the cuts ($R_t : L_c$), to maximize the energy harvested with no HVAC use (Max $\sum_i E_{g_i}$, $HVAC = 0$), to minimize the actuation energy with no HVAC use (Min $\sum_i E_{ci}$, $HVAC = 0$), and to maximize the net energy generated (Max $\sum_i(E_{gi} - E_{ci})$) for the base design date for a single story building scenario in Pittsburgh (note that the colors for each objective match those used for Figure 11).

Objective	N_l	N_t	$R_t : L_c$
Max $\sum_i E_{g_i}$, $HVAC = 0$	15	10	1 : 8
Min $\sum_i E_{ci}$, $HVAC = 0$	25	10	1 : 8
Max $\sum_i(E_{gi} - E_{ci})$	15	10	1 : 8

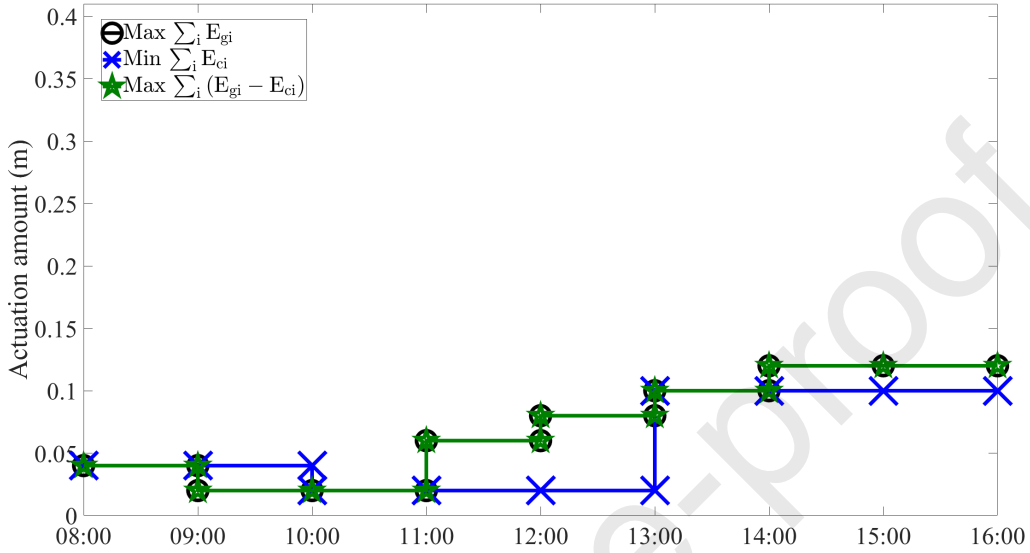

Figure 11: The amount of actuation at each hour for the kirigami-inspired component with the corresponding cut designs given in Table 1 to maximize the energy harvested with no HVAC use (Max $\sum_i E_{g_i}$, $HVAC = 0$), to minimize the actuation energy with no HVAC use (Min $\sum_i E_{ci}$, $HVAC = 0$), and to maximize the net energy generated (Max $\sum_i(E_{gi} - E_{ci})$) for the base design date for a single story building scenario in Pittsburgh (note that the colors for each objective match those used for Table 5).

Table 6: The average air changes per hour (A_h), the total energy harvested (E_g), the total actuation cost (E_c), and the net energy generated (E_t) to maximize the energy harvested with no HVAC use (Max $\sum_i E_{g_i}$, $HVAC = 0$), to minimize the actuation energy with no HVAC use (Min $\sum_i E_{ci}$, $HVAC = 0$), and to maximize the net energy generated (Max $\sum_i(E_{gi} - E_{ci})$) for the base design date for a single story building scenario in Pittsburgh (note that the colors for each objective match those used for Table 5).

Objective	A_h	$E_g(W)$	$E_c(W)$	$E_t(W)$
Max $\sum_i E_{g_i}$	14.3	4532	20	4512
Min $\sum_i E_{ci}$	13.6	3974	12	3964
Max $\sum_i(E_{gi} - E_{ci})$	14.3	4532	20	4512

Table 7: The dates identified to represent the variation in environmental conditions throughout the year 2023 for Pittsburgh, as well as the corresponding range of dates represented and the temperature at the start (8:00), middle (12:00), and end (16:00) of the evaluation period for each date.

Date	**Date Range**	**Temperature at 8:00** ($^\circ C$)	**Temperature at 12:00** ($^\circ C$)	**Temperature at 16:00** ($^\circ C$)
April 5	3/20 to 4/11	19.4	25.6	28.9
April 19	4/12 to 5/5	3.3	10.6	17.8
May 18	5/6 to 5/28	7.2	17.8	22.8
June 18	5/29 to 6/21	12.8	23.9	27.2
July 20	6/22 to 8/6	14.4	25.6	27.8
September 16	8/7 to 9/23	9.4	20.0	23.9
October 2	9/24 to 10/15	15.0	22.8	27.2
October 27	10/16 to 11/6	16.7	20	22.2
November 13	11/7 to 11/29	0.0	12.8	14.4
December 16	11/30 to 12/21	−2.2	7.8	12.8
January 11	12/22 to 1/12	−1.1	4.4	8.3
January 16	1/13 to 2/3	−5.6	2.2	6.7
February 7	2/4 to 2/25	−1.1	10	13.3
March 1	2/26 to 3/19	2.2	18.3	22.2

Diego. Lastly, the cut design parameters to minimize the actuation cost were also the same for Pittsburgh and San Diego, since this set of parameters requires the least work to actuate, and so it can be adjusted with the least amount of energy cost to maintain sufficient air changes and the internal temperature without HVAC use.

For Pittsburgh, 14 days were identified to represent the year 2023, as shown in Table 7, and again the cut parameters identified to maximize the net energy ($N_l = 15$, $N_t = 10$, $R_t : L_c = 1 : 8$) were considered for each day. Table 8 shows the environmental performance of the 14 representative days for the optimized actuation sequence. As would be expected, the larger annual and daily temperature variations in Pittsburgh resulted in even more variation in the performance measures throughout the year than in San Diego. In particular, the ranges of both net energy generated and air changes are more than 20% greater for Pittsburgh than San Diego. Moreover, the more extreme temperatures in Pittsburgh result in several days with simultaneously lower air changes and solar energy harvested than any date for San Diego. However, there are multiple days in Pittsburgh that were operated with zero HVAC use. This is because the generally lower clearness index in Pittsburgh reduces the potential solar energy harvested on most days, so that there is more energy benefit in limiting the component opening, and ultimately preventing the need for HVAC use, than there is to improve the solar tracking and energy harvesting potential.

The weighted sum estimate of the total net energy for the year in Pittsburgh is considerably lower than for San Diego at $1.17MW$, which is an average daily amount of $3215W$ (i.e., approximately 17.02% lower than San Diego). To provide context, a baseline flat and closed façade system would be estimated to net approximately $0.93MW$ over the year ($2548W$ on average per day) for the location in Pittsburgh. As such, even with the larger variability of the performance in Pittsburgh, the active component still produces a relatively large amount of energy gain approximately 20.51% greater than a baseline system. While the increase in performance when compared to a baseline flat façade is lower than San Diego, the façade still falls within the range that is to be expected from an adaptive façade.

The weighted daily average of air changes per hour over the year was estimated to be approximately 20% lower than that for San Diego, but still relatively high at 11.4. Even the minimum air changes for Pittsburgh was 5.7, which is more than double the recommended minimum, again noting air changes were not an optimization objective and simply an added benefit of the device operation.

4.2.4. Multi-story in Pittsburgh, Pennsylvania, USA

Figures 12 and 13 show the net energy generated and Figures 14 and 15 report the average air changes per hour for each of the representative days at the 2nd, 4th, and 7th floors of the multi-story building, for the actuations that maximize the net energy for each day on each floor using the previously selected cut parameters. Similar changes in performance with respect to floor level as seen for San Diego can be observed for the multi-story building in Pittsburgh, including the noted complexity of the relationship between performance and the building and environmental conditions. For example, one day that had increasing performance metrics with floor height in Pittsburgh was October 27th, which has a similar outdoor temperature as June 20th in San Diego that also had increasing metrics with height. Alternatively, consistently warmer or colder days generally had decreasing performance metrics with height, similarly to the results in San Diego.

There is a significantly larger floor-to-floor variation in performance in Pittsburgh than in San Diego, with the average floor-to-floor change in energy and air change performance of $74.62W$ and 1.76 and the standard deviations were 68.0 W and 1.41, respectively. Moreover, a major difference between the two locations is that 5 out of the 14 days considered in Pittsburgh had no air changes for higher floors, since these days are too cold and either the capacity of the HVAC would be exceeded or the HVAC use would be so high that not opening the component would still result in more net energy. The component being required to be closed also means that the component is not able to track the sun for improved solar harvesting at those times. As such, higher floors would not benefit year-round from the façade concept in Pittsburgh.

The weighted sum estimate of the total annual net energy for the multi-story building in Pittsburgh is 6.80 MW, which is an average daily amount of 18.6 KW, and the weighted daily average of air changes per hour over the year is 6.33. Therefore, the energy

Table 8: The average air changes per hour (A_h), the total energy harvested (E_g), the total actuation cost (E_c), the energy cost required to use the HVAC (HVAC), and the net energy generated (E_t) for the cut design that maximized net energy generated for the base design date and with an actuation sequence that maximized net energy generated for each representative date for the year 2023 for the single story building scenario in San Diego.

Date	A_h	$E_g(W)$	$E_c(W)$	$HVAC(W)$	$E_t(W)$
April 5	17.9	4771	18	1217	3536
April 19	11.2	4255	42	0	4213
May 18	11.6	4513	18	378	4117
June 18	11.6	4454	21	492	3941
July 20	10.2	4649	23	924	3702
September 16	14.8	3849	19	312	3518
October 2	13.5	3539	18	694	2827
October 27	15.9	2972	23	442	2507
November 13	7.9	2487	24	0	2463
December 16	7.8	2418	20	0	2398
January 11	6.9	2385	8	113	2264
January 16	5.7	2427	16	122	2289
February 7	8.3	2882	15	0	2867
March 1	11.5	3468	20	226	3222

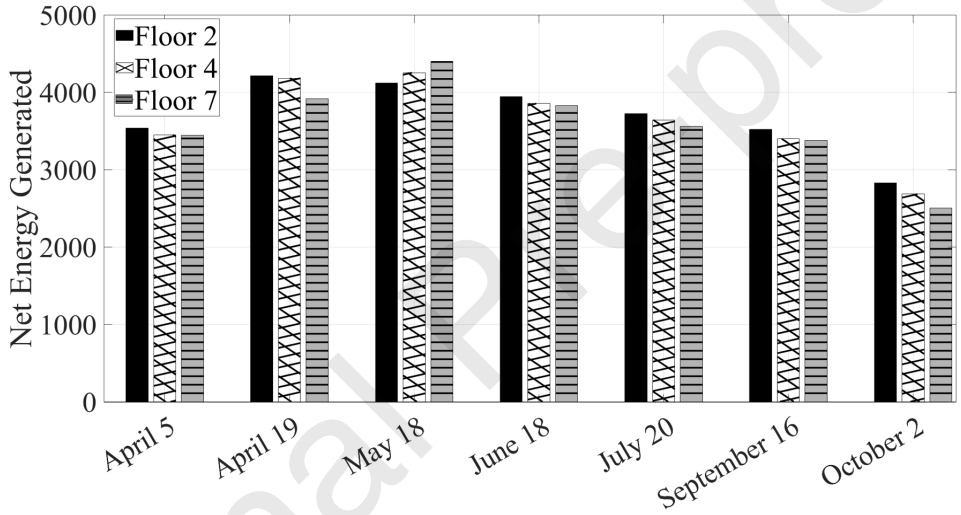

Figure 12: The average air changes per hour for floor 2 (black), floor 4 (white with cross hatching), and floor 7 (grey with horizontal lines) for the cut design that maximized net energy generated for the base design date and with an actuation sequence that maximized net energy generated for the first half of the representative dates for the year 2023 for the single story building scenario in Pittsburgh.

performance of the building scales similarly as well as in San Diego, with the 6 active floors producing 5.81 times more energy than the estimated performance of 1 active floor. However, the average air changes over the year for all floors is 42.97% less for the multi-story system compared to the single story. Thus, while the energy performance is relatively consistent for both San Diego and Pittsburgh, the ventilation performance decreases substantially for multi-story systems in a more variable temperature environment such as Pittsburgh.

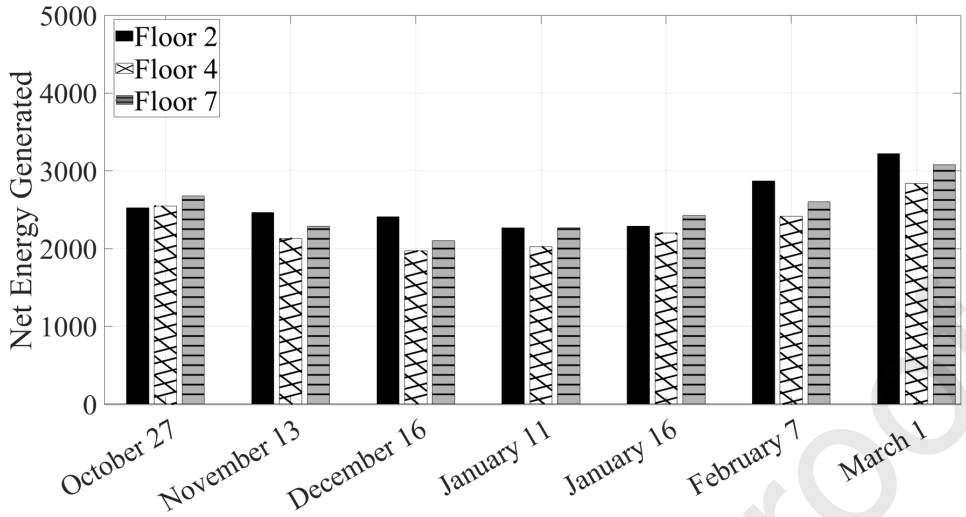

Figure 13: The average air changes per hour for floor 2 (black), floor 4 (white with cross hatching), and floor 7 (grey with horizontal lines) for the cut design that maximized net energy generated for the base design date and with an actuation sequence that maximized net energy generated for the second half of the representative dates for the year 2023 for the single story building scenario in Pittsburgh.

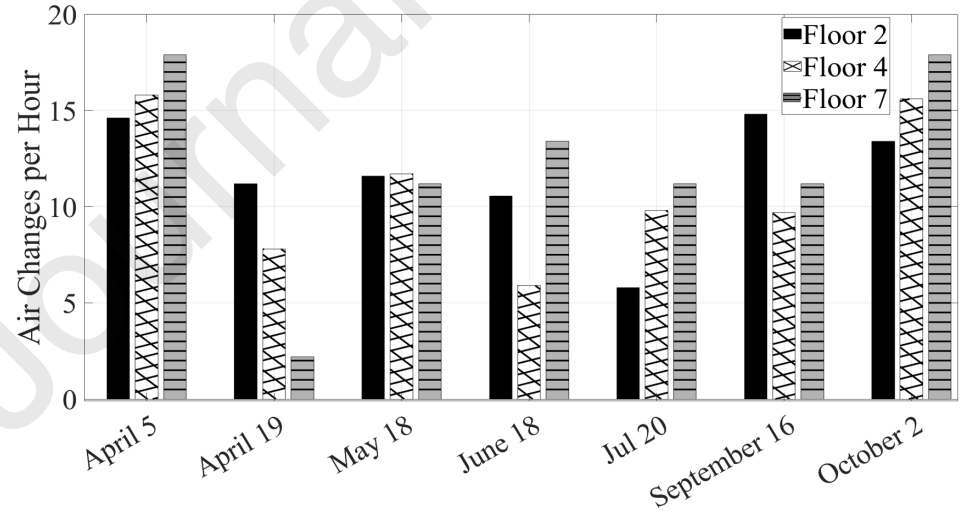

Figure 14: The average air changes per hour for floor 2 (black), floor 4 (white with cross hatching), and floor 7 (grey with horizontal lines) for the cut design that maximized net energy generated for the base design date and with an actuation sequence that maximized net energy generated for the first half of the representative dates for the year 2023 for the single story building scenario in Pittsburgh.

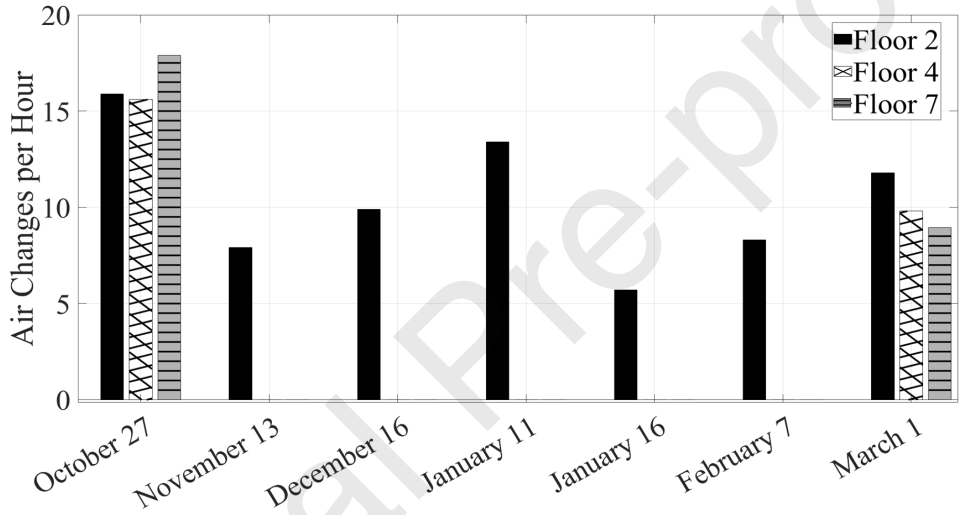

Figure 15: The average air changes per hour for floor 2 (black), floor 4 (white with cross hatching), and floor 7 (grey with horizontal lines) for the cut design that maximized net energy generated for the base design date and with an actuation sequence that maximized net energy generated for the second half of the representative dates for the year 2023 for the single story building scenario in Pittsburgh.

5. Conclusions and Future Directions

A novel kirigami-inspired double-skin façade concept was presented and evaluated. The key feature of this double skin concept is the incorporation of a kirigami-inspired component on the outer skin, which can be actuated to open the cut portions of the component facilitating adaptive ventilation, while the regions of the component around the cuts rotate to facilitate solar tracking. While such a system could achieve a range of environmental interaction objectives, the present study focused on the potential to apply this technology to simultaneously improve air changes and reduce HVAC cost to maintain temperature in an associated indoor space and harvest solar energy with embedded solar panels. A numerical approach to estimate performance was presented and a set of computational case studies were used to evaluate the potential performance of the proposed façade concept as part of a building system. The case studies considered various building scenarios, including differing building sizes, geographic locations, environmental conditions, and duration of operation.

The façade concept was shown to increase environmental performance of the buildings for a wide range of outdoor temperatures and wind speeds by decreasing HVAC use and in some cases eliminating the need for HVAC entirely. As expected when there is some heat generation (e.g., people and/or equipment) within the associated space, ventilation-based HVAC assistance such as this is particularly effective when the outdoor temperature is slightly lower than the desired indoor temperature, and higher wind speed leads to increased effectiveness when the outdoor temperatures are higher. However, the net energy performance of the façade concept is beneficial even with outdoor temperatures ranging above or well below the desired internal temperature when considering adaptive usage on a building throughout a day. Overall, the component cut design parameters can have a significant impact on the potential environmental performance, as differing objective preferences (e.g., maximizing solar energy harvesting versus minimizing HVAC energy cost) produce different optimal cut design parameters. Yet, there can be significant net energy performance increase for a building in a wide range of environmental conditions (e.g., San Diego or Pittsburgh) and durations (e.g., 1 day or 1 year) due to the adaptivity, in comparison to a standard flat closed façade.

Although the potential environmental performance of the proposed kirigami-inspired double-skin adaptive facade concept was established, several practical considerations remain to be addressed towards translation from research to practice. Future work should naturally include development and testing of device prototypes, to answer the questions related to materials selection, hardware selection, and overall component configuration, as well as further refinement and validation of the computational strategies to estimate performance to better design and operate the device once implemented. Establishing such details

likely leads to more comprehensive analysis as well, including consideration of environmental impacts, fabrication, maintenance and durability, and/or overall sustainability estimation.

Declaration of competing interest

The authors declare that they have no known competing financial interests or personal relationships that could have appeared to influence the work reported in this paper.

Data availability

Data will be made available on request.

Support acknowledgement and disclaimer

This material is based upon work supported by the National Science Foundation under Grant No. 2332246 and Grant No. 2329758

References

[1] Dat Tien Doan, Ali Ghaffarianhoseini, Nicola Naismith, Tongrui Zhang, Amirhosein Ghaffarianhoseini, and John Tookey. A critical comparison of green building rating systems. *Building and Environment*, 123:243–260, 2017.

[2] Daniel Uribe, Sergio Vera, Waldo Bustamante, Andrew McNeil, and Gilles Flamant. Impact of different control strategies of perforated curved louvers on the visual comfort and energy consumption of office buildings in different climates. *Solar Energy*, 190:495–510, 2019.

[3] Silvia Cesari, Paolo Valdiserri, Maddalena Coccagna, and Sante Mazzacane. The energy saving potential of wide windows in hospital patient rooms, optimizing the type of glazing and lighting control strategy under different climatic conditions. *Energies*, 13(8):2116, 2020.

[4] Andrew Kusiak, Mingyang Li, and Fan Tang. Modeling and optimization of hvac energy consumption. *Applied Energy*, 87(10):3092–3102, 2010.

[5] Flemming Abrahamsen, Frede Blaabjerg, John K Pedersen, Pawel Z Grabowski, and Paul Thogersen. On the energy optimized control of standard and high-efficiency induction motors in ct and hvac applications. *IEEE Transactions on Industry Applications*, 34(4):822–831, 1998.

[6] Yasin Kabalci. A survey on smart metering and smart grid communication. *Renewable and Sustainable Energy Reviews*, 57:302–318, 2016.

[7] Paula Rocha, Afzal Siddiqui, and Michael Stadler. Improving energy efficiency via smart building energy management systems: A comparison with policy measures. *Energy and Buildings*, 88:203–213, 2015.

[8] NM Nahar, Paban Sharma, and MM Purohit. Performance of different passive techniques for cooling of buildings in arid regions. *Building and Environment*, 38(1):109–116, 2003.

[9] MS Hatamipour and A Abedi. Passive cooling systems in buildings: some useful experiences from ancient architecture for natural cooling in a hot and humid region. *energy conversion and management*, 49(8):2317–2323, 2008.

[10] WJ Hee, MA Alghoul, Ba Bakhtyar, OmKalthum Elayeb, MA Shameri, MS Alrubaih, and K Sopian. The role of window glazing on daylighting and energy saving in buildings. *Renewable and Sustainable Energy Reviews*, 42:323–343, 2015.

[11] NBI Rasli, NA Ramli, NM Kamaruddin, MB Salleh, ABDELRAHMAN Ismail, and MOHD RODZI Ismail. A qualitative study on airflow characteristics across a wooden slotted down window panel for passive ventilation and façade shading application. *Journal of Sustainability Science and Management*, 16(4):124–136, 2021.

[12] Jan Zajas and Per Heiselberg. Analysis of energy saving potential and optimization of thermally broken fiberglass window frames. In *Proceedings of the 12th Conference of International Building Performance Simulation Association, Sydney, Australia*, pages 14–16, 2011.

[13] Ri Na and Zhigang Shen. Assessing cooling energy reduction potentials by retrofitting traditional cavity walls into passively ventilated cavity walls. In *Building Simulation*, volume 14, pages 1295–1309. Springer, 2021.

[14] Ziyi Su, Xiaofeng Li, and Fei Xue. Double-skin façade optimization design for different climate zones in china. *Solar Energy*, 155:281–290, 2017.

[15] Zhongting Hu, Wei He, Jie Ji, and Shengyao Zhang. A review on the application of trombe wall system in buildings. *Renewable and Sustainable Energy Reviews*, 70:976–987, 2017.

[16] I Guedi Capeluto. Energy performance of the self-shading building envelope. *Energy and buildings*, 35(3):327–336, 2003.

[17] Amir Tabadkani, Astrid Roetzel, Hong Xian Li, and Aris Tsangrassoulis. Design approaches and typologies of adaptive facades: A review. *Automation in Construction*, 121:103450, 2021.

[18] Rana Abdollahi Rizi and Ahmad Eltaweel. A user detective adaptive facade towards improving visual and thermal comfort. *Journal of Building Engineering*, 33:101554, 2021.

[19] Seyed Morteza Hosseini, Masi Mohammadi, Alexander Rosemann, Torsten Schröder, and Jos Lichtenberg. A morphological approach for kinetic façade design process to improve visual and thermal comfort. *Building and environment*, 153:186–204, 2019.

[20] Kyounghee Kim and C Jerratt. Energy performance of an adaptive façade system. *J. Archit. Res*, pages 179–186, 2011.

[21] Daniel Aelenei, Laura Aelenei, and Catarina Pacheco Vieira. Adaptive façade: concept, applications, research questions. *Energy Procedia*, 91:269–275, 2016.

[22] Mohanned Al Thobaiti. *Intelligent and Adaptive Façade System: The Impact of Intelligent and Adaptive Façade on The Performance and Energy Efficiency of Buildings*. PhD thesis, University of Miami, 2014.

[23] RCGM Loonen. Approaches for computational performance optimization of innovative adaptive façade concepts. 2018.

[24] Jens Boeke, Ulrich Knaack, and Marco Hemmerling. Superposition matrix for the assessment of performance-relevant adaptive façade functions. *Journal of Facade Design and Engineering*, 7(2):1–20, 2019.

[25] Laura Elena Aelenei, Daniel Aelenei, Rosa Romano, Enrico Sergio Mazzucchelli, Marcin Brzezicki, and Jose Miguel Rico-Martinez. Case studies: adaptive facade network, 2018.

[26] Dac-Khuong Bui, Tuan Ngoc Nguyen, Abdallah Ghazlan, Ngoc-Tri Ngo, and Tuan Duc Ngo. Enhancing building energy efficiency by adaptive façade: A computational optimization approach. *Applied energy*, 265:114797, 2020.

[27] Riham Nady. Dynamic facades: environmental control systems for sustainable design. *Renewable Energy and Sustainable Development*, 3(1):118–127, 2017.

[28] Scott Charles Murray. *Contemporary curtain wall architecture*. Princeton Architectural Press, 2009.

[29] Jozef Hraska. Adaptive solar shading of buildings. *International Review of Applied Sciences and Engineering*, 9(2):107–113, 2018.

[30] Shady Attia. Evaluation of adaptive facades: The case study of al bahr towers in the uae. *QScience Connect*, 2017(2):6, 2017.

[31] Rishika Sood and Anjali S Patil. Analysis and review of the kinetic façades in kolding campus, south denmark university. *Artificial Intelligence and Sustainable Computing: Proceedings of ICSISCET 2020*, pages 265–274, 2021.

[32] Faysal M Abo Elazm and Basma S Saad. Towards novel and appropriate smart buildings "beijing water cube. *International Journal of Education and Learning Systems*, 2, 2017.

[33] Marco Meloni, Qian Zhang, Jianguo Cai, and Daniel Sang-Hoon Lee. Origami-based adaptive facade for reducing reflected solar radiation in outdoor urban environments. *Sustainable Cities and Society*, page 104740, 2023.

[34] Mahdi Valitabar, Ali GhaffarianHoseini, Amirhosein GhaffarianHoseini, and Shady Attia. Advanced control strategy to maximize view and control discomforting glare: a complex adaptive façade. *Architectural engineering and design management*, 18(6):829–849, 2022.

[35] Robert Joseph Zupan, Dale Clifford, Richard Beblo, and John Brigham. Numerical investigation of capabilities for dynamic self-shading through shape changing building surface tiles. *Journal of Facade Design and Engineering*, 6(1):57–69, 2018.

[36] Matteo Iommi. The mediterranean smart adaptive wall. an experimental design of a smart and adaptive facade module for the mediterranean climate. *Energy and Buildings*, 158:1450–1460, 2018.

[37] Ainagul Jumabekova, Julien Berger, Tessa Hubert, Antoine Dugué, Tingting Vogt Wu, Thomas Recht, and Christian Inard. A state-space model to

control an adaptive facade prototype using data-driven techniques. *Energy and Buildings*, page 113391, 2023.

[38] Robert J Zupan, Jing Xu, Richard V Beblo, Dale T Clifford, Ankush Aggarwal, and John C Brigham. Computational design optimization of a smart material shape changing building skin tile. *Engineering Structures*, 201:109839, 2019.

[39] Robert J Zupan, Dale T Clifford, Richard V Beblo, and John C Brigham. Design, prototyping, and evaluation of a concept for a shape-changing smart material building surface tile. *Smart Materials and Structures*, 29(11):115052, 2020.

[40] Siliang Yang, Francesco Fiorito, Alistair Sproul, and Deo Prasad. Optimising design parameters of a building-integrated photovoltaic double-skin facade in different climate zones in australia. *Buildings*, 13(4):1096, 2023.

[41] Irina Leonidovna Vasileva, Darya Viktorovna Nemova, Nikolai Ivanovich Vatin, Roman Sergeevich Fediuk, and Maria Iurevna Karelina. Climate-adaptive façades with an air chamber. *Buildings*, 12(3):366, 2022.

[42] Jan Hensen, Martin Bartak, and Frantisek Drkal. Modeling and simulation of a double-skin facade system. *ASHRAE transactions*, 108(2):1251–1259, 2002.

[43] Elena Catto Lucchino and Francesco Goia. Multi-domain model-based control of an adaptive façade based on a flexible double skin system. *Energy and Buildings*, 285:112881, 2023.

[44] Rodrigo Arauz, Aminallah Pourasghar, and John C Brigham. Evaluation of the effects of cut design parameters on the environmental performance of a kirigami-inspired façade concept. *Energy and Buildings*, page 113432, 2023.

[45] Yaxing Li, Kai Chang, Jingyu Chang, Boyang Yu, Linna Liu, Bingyang Liu, Xinyan Zhao, and Weiwei Deng. Printed kirigami organic photovoltaics for efficient solar tracking. *Advanced Functional Materials*, 32(34):2204004, 2022.

[46] Wenting Ding, Yuji Hasemi, and Tokiyoshi Yamada. Natural ventilation performance of a double-skin façade with a solar chimney. *Energy and buildings*, 37(4):411–418, 2005.

[47] Cynthia Howard-Reed, Lance A Wallace, and Wayne R Ott. The effect of opening windows on air change rates in two homes. *Journal of the Air & Waste Management Association*, 52(2):147–159, 2002.

[48] F Marques da Silva, M Glória Gomes, and A Moret Rodrigues. Measuring and estimating airflow in naturally ventilated double skin facades. *Building and Environment*, 87:292–301, 2015.

[49] Y Ji, MJ Cook, Victor Ian Hanby, DG Infield, DL Loveday, and L Mei. Cfd modelling of double-skin facades with venetian blinds. *Building Simulation 2007*, pages 1491–1498, 2007.

[50] Nassim Safer, Monika Woloszyn, and Jean Jacques Roux. Three-dimensional simulation with a cfd tool of the airflow phenomena in single floor double-skin facade equipped with a venetian blind. *Solar Energy*, 79(2):193–203, 2005.

[51] Wilmer Pasut and Michele De Carli. Evaluation of various cfd modelling strategies in predicting airflow and temperature in a naturally ventilated double skin façade. *Applied Thermal Engineering*, 37:267–274, 2012.

[52] Ahmet Vefa Orhon. 0171—a review on adaptive photovoltaic façades. In *Proceedings of the Solar TR2016 International Solar Conference & Exhibition, Istanbul, Turkey*, pages 6–8, 2016.

[53] Aaron Lamoureux, Kyusang Lee, Matthew Shlian, Stephen R Forrest, and Max Shtein. Dynamic kirigami structures for integrated solar tracking. *Nature communications*, 6(1):8092, 2015.

[54] John A Duffie, William A Beckman, and Nathan Blair. *Solar engineering of thermal processes, photovoltaics and wind*. John Wiley & Sons, 2020.

[55] ASM International, ASM International. Reference Publications, and American Society for Metals. Reference Publications. *ASM Engineered Materials Reference Book*. ASM International, 1989.

[56] Renogy. Rng-175db-h manual. https://www.renogy.com/content/Manual/RNG-175DB-H.pdf. Accessed: 1-11-2024.

[57] PJ Spaur. *Investigation of discharge coefficients for irregular orifices*. West Virginia University, 2011.

[58] Masoud Karbasi, Mehdi Jamei, Iman Ahmadianfar, and Amin Asadi. Toward the accurate estimation of elliptical side orifice discharge coefficient applying two rigorous kernel-based data-intelligence paradigms. *Scientific Reports*, 11(1):19784, 2021.

[59] Muhammad Iqbal, Akihito Ozaki, Younhee Choi, Yusuke Arima, and Tomoyuki Hamashima. Investigation of discharge coefficient of louvre openings in naturally ventilated buildings. In *E3S Web of Conferences*, volume 396, page 02030. EDP Sciences, 2023.

[60] United States. Occupational Safety, Health Administration. Office of Science, and Technology Assessment. *OSHA Technical Manual*, volume 015. US Department of Labor, Occupational Safety and Health Administration . . . , 2017.

[61] Damla Elbi, Hüma Fulya Ekim, and Onur Dursun. Optimizing natural ventilation strategy in existing buildings using differential evolution: Case of architectural studio classrooms. In *2016 IEEE Congress on Evolutionary Computation (CEC)*, pages 3895–3900. IEEE, 2016.

[62] National Weather Service Glossary. https://forecast.weather.gov/glossary.php. Accessed: 2024-04-06.

[63] Ajaya Kumar Gupta and Peter James Moss. *Guidelines for design of low-rise buildings subjected to lateral forces*. CRC Press, 2020.

[64] Refrigerating American Society of Heating and Air-Conditioning Engineers. Ventilation for acceptable indoor air quality.

[65] Yanhuo Luo. Innovative design of adaptive energy-saving facade of green buildings based on photovoltai colour-changing technology. *International Core Journal of Engineering*, 10(6):19–25, 2024.

[66] Hanan M Taleb and Rudy Moarbes. Improving illuminance performance by implementing a kinetic façade system: case study of office building in dubai. *Journal of Asian Architecture and Building Engineering*, 22(5):2809–2826, 2023.

Evaluation of a Kirigami-Inspired Double-Skin Adaptive Façade for Natural Ventilation and Solar Harvesting to Enhance Indoor Environment and Energy Performance

Kirigami-inspired Double-Skin Façade Concept

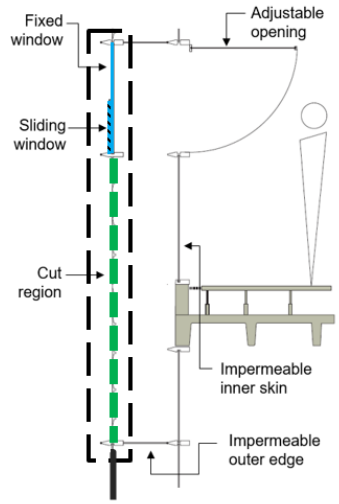

Outer-skin Operation

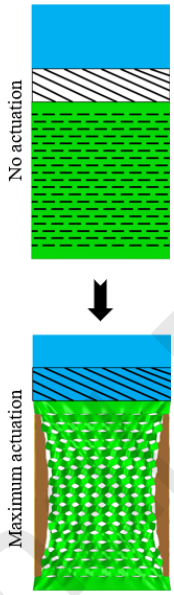

Numerical Evaluation of Building Performance to Enhance Indoor Environment and Energy Generation

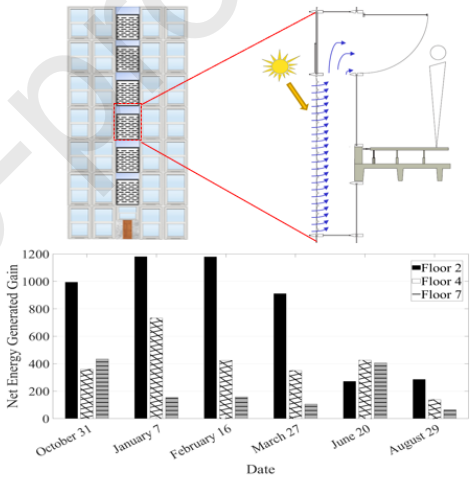

Gain in net energy for the kirigami-inspired façade vs. a flat closed façade by floor of a building on different days of the year.

Conclusions: The component is most effective when the outdoor temperature is near to the desired indoor temperature and wind speeds are mild, but can still reduce HVAC usage for more disparate temperatures. The component has the potential to significantly increase net energy generation, with yearly performance estimated for the scenarios to be as much as 25% greater than that of a flat closed façade.

University of Pittsburgh
Swanson School of Engineering

Arauz, Filipov, Fascetti, Clifford, Brigham, 2024

Declaration of interests

☒ The authors declare that they have no known competing financial interests or personal relationships that could have appeared to influence the work reported in this paper.

☐ The authors declare the following financial interests/personal relationships which may be considered as potential competing interests: